2.5. Two-phase flow model coupled with mechanical deformations within the FE code CODE_BRIGHT (UPC)

Executive Summary

The safest long-term management solution for high-activity radioactive waste is known as geological disposal. Many countries (e.g. Canada, Finland, France, Switzerland, Sweden, UK and USA) have chosen to dispose of all or part of their spent nuclear fuel in facilities constructed at an appropriate depth in stable geological formations. Bentonite based materials have been proposed as engineered barrier system around the canister because of their high retention capacity, high swelling ability and low permeability (Toprak et al., 2020) (Toprak et al., 2020).

In the repository gas will be generated by several mechanisms, such as the anaerobic corrosion of metals, the microbial degradation of organic wastes and the radiolysis of water, which generate hydrogen, oxygen, methane and carbon dioxide. In the case of the engineer barriers, gas transport could take place mainly through preferential pathways, like the joints between compacted bentonite blocks, interfaces between different components or along the interface between host rock and buffer material. After the complete saturation of the barrier, gas generated will increase up to a locally defined threshold or breakthrough pressure, from which gas flow will take place through temporary pathways. Once breakthrough pressure is reached, preferential pathways will be created. The size of these pathways would depend on gas local pressure and structural clay restrictions. These pathways would close once gas pressure decrease below a certain value, known as residual pressure. Meanwhile, gas pressure will increase again at the interface up to a new threshold pressure. Therefore, the gas generated will be transported outwards in a cyclic manner, regulated by the opening and closure of pathways, which will depend on the pressure reached (Gutiérrez Rodrigo, 2019).

In order to investigate gas migration from bentonite barrier (FEBEX bentonite) and gas pathway development along the barrier; hydro-mechanical simulations of breakthrough tests on FEBEX material (Gutiérrez Rodrigo, 2019) have been performed.

2.5.1. Model introduction

Gas diffusion, two-phase flow and two-phase flow coupled with mechanical effects are some of mechanisms for gas transport that may lead to generation of apertures (small fractures) in the porous medium. Due to low permeability of EBS components, the air entry pressure is higher. Therefore, a higher capillary pressure is needed for the desaturation of clay based material during gas injection.

Under a certain rate of gas generation, the gas pressure may increase and once reaching values of BT, gas fracture processes will begin. Alternatively, through gas generation, gas may flow through existing discontinuities (Olivella et al., 1994). In order to take into account fracture opening and/or fracture formation because of gas generation a proper mechanical model is required.

In this work, a standard two-phase flow model has been used to simulate gas breakthrough tests on FEBEX material. The flow model is coupled to mechanical deformation. During gas injection, gas flow pathways develops (Figure 2.102). It is a continuous model where apertures have cubic law for permeability (Olivella and Alonso, 2008a).Generated gas is transported in a cyclic manner, regulated by the opening and closure of pathways.

Permeability increases during gas injection because of aperture of the fractures and reduces during closure of these apertures. Basic features of the model such as permeability coupled to mechanical behaviour

evolution of intrinsic permeability according to deformation rate (Olivella and Alonso, 2008a) and its impact on pathway development are shown in Figure 2.102. Hydro-mechanical models' equations and parameters are summarized from Table 2.22 to Table 2.25. Equations for the advective and dissolved non-advective gas flow can be found in details in (Olivella and Alonso, 2008a) and Olivella et al., 1994 (Olivella et al., 1994).

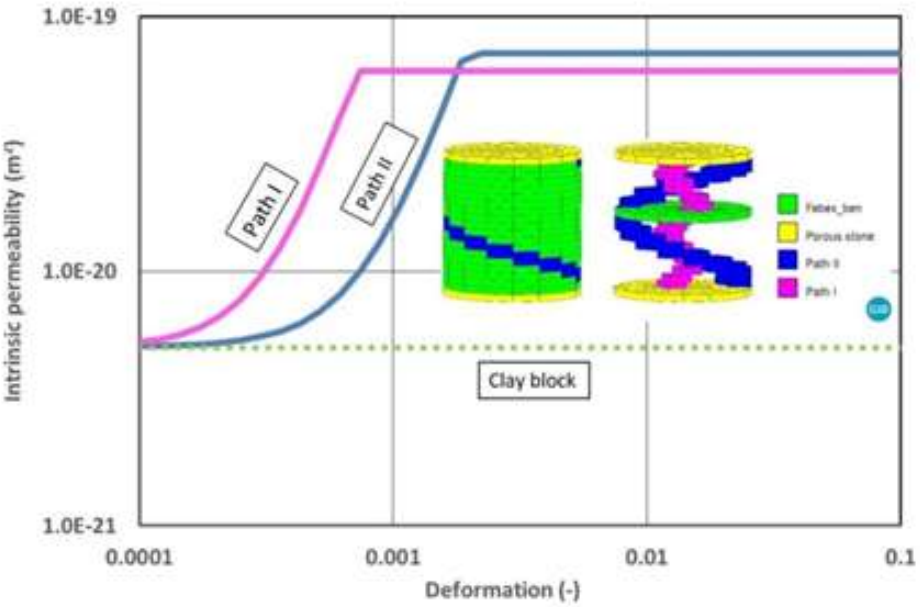

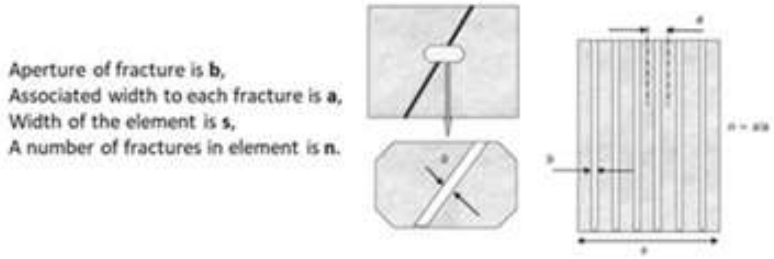

$$k_{\text{int}} = k_{\text{matrix}} + k_{\text{fractures}}$$

$$k_{\text{fractures}} = \frac{b^3}{12a}, \quad b = b_0 + \langle \varepsilon - \varepsilon_0 \rangle a \leq b_{\max}$$

Figure 2.102: Relationship between intrinsic permeability and deformation in the Model. Cubic law for permeability used for preferential paths.

Laws	Parameter	Units	Symbol	Equations
Van Genuchten retention curve	Capillary pressure parameter (in P(ϕ)) Shape parameter in $\lambda(\phi)$ Maximum saturation	(MPa) (–) (–)	P_0 λ_0 S_{ls}	$S_l = \left(1 + \left(\frac{p_g - p_l}{P}\right)^{\frac{1}{1-\lambda}}\right)^{-\lambda}$
Advective Darcy flux	Reference intrinsic permeability Reference porosity Initial porosity	(m^2) (–) (–)	k_0 ϕ_0 ψ	$\mathbf{q}_l = -\frac{\mathbf{k}k_{rl}}{\mu_l}(\nabla p_l + \rho_l g \nabla z)$ $\mathbf{k} = \mathbf{k}_0 \frac{\psi^3}{(1-\psi)^2}\frac{(1-\psi_0)^2}{\psi_0^3}$
Gas relative permeability	Gas relative permeability – constant Gas relative permeability – power Maximum gas saturation – power	(–) (–) (–)	A λ S_{gs}	$k_{rl} = AS_{eg}^{\lambda}$ $S_{eg} = \frac{S_g - S_{rg}}{S_{gs} - S_{rg}}$
Cubic law for permeability	Initial aperture to calculate a variable aperture Spacing of the fractures: Reference strain to calculate aperture variations Maximum aperture. Upper bound of aperture.	(m) (m) (–) (m)	b_0 a ε_0 b_{max}	$b = b_0 + \Delta b$ $k = k_{max} + \frac{b^3}{12a}$ $\Delta b = a\Delta\varepsilon = a(\varepsilon - \varepsilon_0)$ for $\varepsilon > \varepsilon_0$

Table 2.22: Constitutive equations for hydraulic laws used in the model

Equation	Parameter	Units	Symbol	FEBEX	Path I	Path II
Van Genuchten retention curve	Capillary pressure parameter (in P(ϕ)) Shape parameter in $\lambda(\phi)$ Maximum saturation	(MPa) (–) (–)	P_0 λ_0 Sls	20 0.18 1	20 0.18 1	20 0.18 1
Advective Darcy flux	Reference intrinsic permeability Reference porosity Initial porosity	(m^2) (–) (–)	k_0 ϕ_0 ψ	5×10^{-21} 0.33 0.33	5×10^{-21} 0.33 0.33	5×10^{-21} 0.33 0.33
Gas relative permeability	Gas relative permeability – constant Gas relative permeability – power Maximum gas saturation – power	(–) (–) (–)	A λ Sgs	100 3 1	100 3 1	100 3 1
Cubic law for permeability	Initial aperture to calculate a variable aperture Spacing of the fractures: Reference strain to calculate aperture variations Maximum aperture. Upper bound of aperture.	(m) (m) (–) (m)	b_0 a ε_0 b_{max}	– – – –	1×10^{-9} 1×10^{-5} 1×10^{-6} 2×10^{-8}	1×10^{-9} 4×10^{-5} 1×10^{-6} 3×10^{-8}
Diffusive Fick flux	Tortuosity coefficient	(–)	τ	0.8	0.8	0.8

Table 2.23: Hydraulic parameters of materials.

Most of the mechanical model (BBM) parameters have been derived from Alonso et al. (1990) and Gens et al. (2009). Back analyses of a swelling pressure test on FEBEX material has been performed in order to calibrate some of BBM parameters listed in Table 2.25. More details about FEBEX material can be found in (Enresa,2000) (Enresa, 2000) and (Enresa,2006) (Enresa, 2006).

Calibration of gas permeability is shown in Figure 2.103 . Water retention curve, LC curve and *s*-p_{eff}-*q* path for the clay are shown in Figure 2.104. Sensitivity analyses have been performed on these parameters in Chapter 3.

2.5.2. Initial Calculations

GID as a CAD system and Code_Bright as a Finite Element Method (FEM) program have been used in order to simulate gas breakthrough test (Gutiérrez Rodrigo, 2019) (laboratory scale – Figure 2.105) on FEBEX bentonite material.

Parameters	Units	Symbol	Equations
Parameters for elastic volumetric compressibility against mean net stress change	(–)	κ_{i0}	$d\varepsilon_v^e = \frac{\kappa_i(s)}{1+e}\frac{dp'}{p'} + \frac{\kappa_s(p',s)}{1+e}\frac{ds}{s+0.1}$
Parameters for elastic volumetric compressibility against suction change	(–)	κ_{s0}	
Minimum bulk modulus Poisson ratio	(MPa) (–)	K_{min} ν	$K = \frac{1+e}{\kappa}p'$, $G = \frac{3K(1-2\nu)}{2(1+\nu)}$
Slope of void ratio – mean net stress curve at zero suction	(–)	$\lambda(0)$	$p_0 = p^c\left(\frac{p_0^*(T)}{p^c}\right)^{\frac{\lambda(0)-\kappa_{i0}}{\lambda(s)-\kappa_{i0}}}$
Parameters for the slope void ratio mean net stress at variable suction	(–) (MPa^{-1})	r β	$\lambda(s) = \lambda(0)\left[(1-r)\exp(-\beta s) + r\right]$
Parameter for increase of tensile strength due to suction	(–)	k	$p_s = p_{s0} + ks\ \exp(-\rho\Delta T)$
Tensile strength in saturated conditions Reference pressure for the p_0 function Critical state line Non-associativity parameter	(MPa) (MPa) (–) (–)	p_{s0} p_c M α	$G = q^2 - \alpha M^2\left(p' + p_s\right)\left(p_0 - p'\right)$
Initial void ratio Pre-consolidation mean stress for saturated soil	(–) (MPa)	ε_0 $p*_0$	$dp_0^* = \frac{1+e}{\lambda(0)-\kappa_{i0}}p_0^* d\varepsilon_v^p$

Table 2.24: Constitutive equations for mechanical law used in the model.

Parameters	Units	Symbol	FEBEX
Parameters for elastic volumetric compressibility against mean net stress change	(–)	κ_{i0}	0.04
Parameters for elastic volumetric compressibility against suction change	(–)	κ_{s0}	0.03
Minimum bulk modulus	(MPa)	K_{min}	10
Poisson ratio	(–)	ν	0.4
Slope of void ratio – mean net stress curve at zero suction	(–)	$\lambda(0)$	0.15
Parameters for the slope void ratio mean net stress at variable suction	(–)	r	0.925
	(MPa^{-1})	β	0.1
Parameter for decrease of tensile strength due to temperature	($°C^{-1}$)	ρ	0.2
Parameter for increase of tensile strength due to suction	(–)	k	0.1
Tensile strength in saturated conditions	(MPa)	p_{s0}	0.1
Reference pressure for the p_0 function	(MPa)	p_c	0.5
Critical state line	(–)	M	1
Non-associativity parameter	(–)	α	0.53
Initial void ratio	(–)	ε_0	0.66
Pre-consolidation mean stress for saturated soil	(MPa)	$p*_0$	12

Table 2.25: Mechanical parameters for materials.

Model A and Model B correspond to arbitrary realization of heterogeneity assuming some preferential paths (A and B) and some random heterogeneous zones (B). In the future, more realizations should be done to analyse the response depending on the distribution of properties.

The sample (FEBEX bentonite) diameter is 38 mm and initial height of the sample is 20 mm. Initial saturation degree of the material is 81% which corresponds to initial water content of 15.3%. The test has been performed under constant volume.

The model has a 3D full geometry where porous stones have been simulate as separate materials. The geometry has structured mesh and the number of hexahedra elements is 960. There are 1197 nodes.

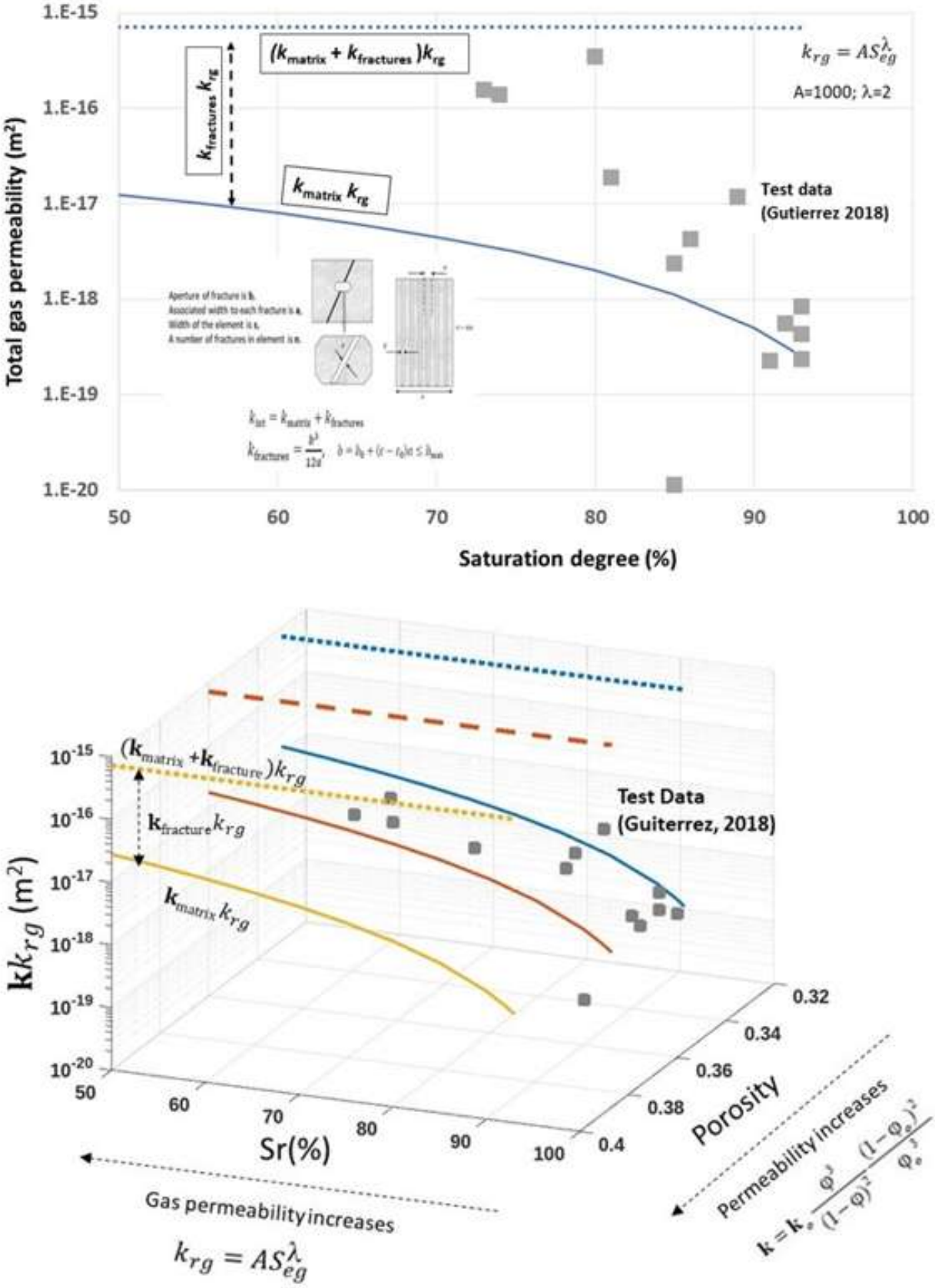

Figure 2.103: Calibration of total gas permeability parameters.

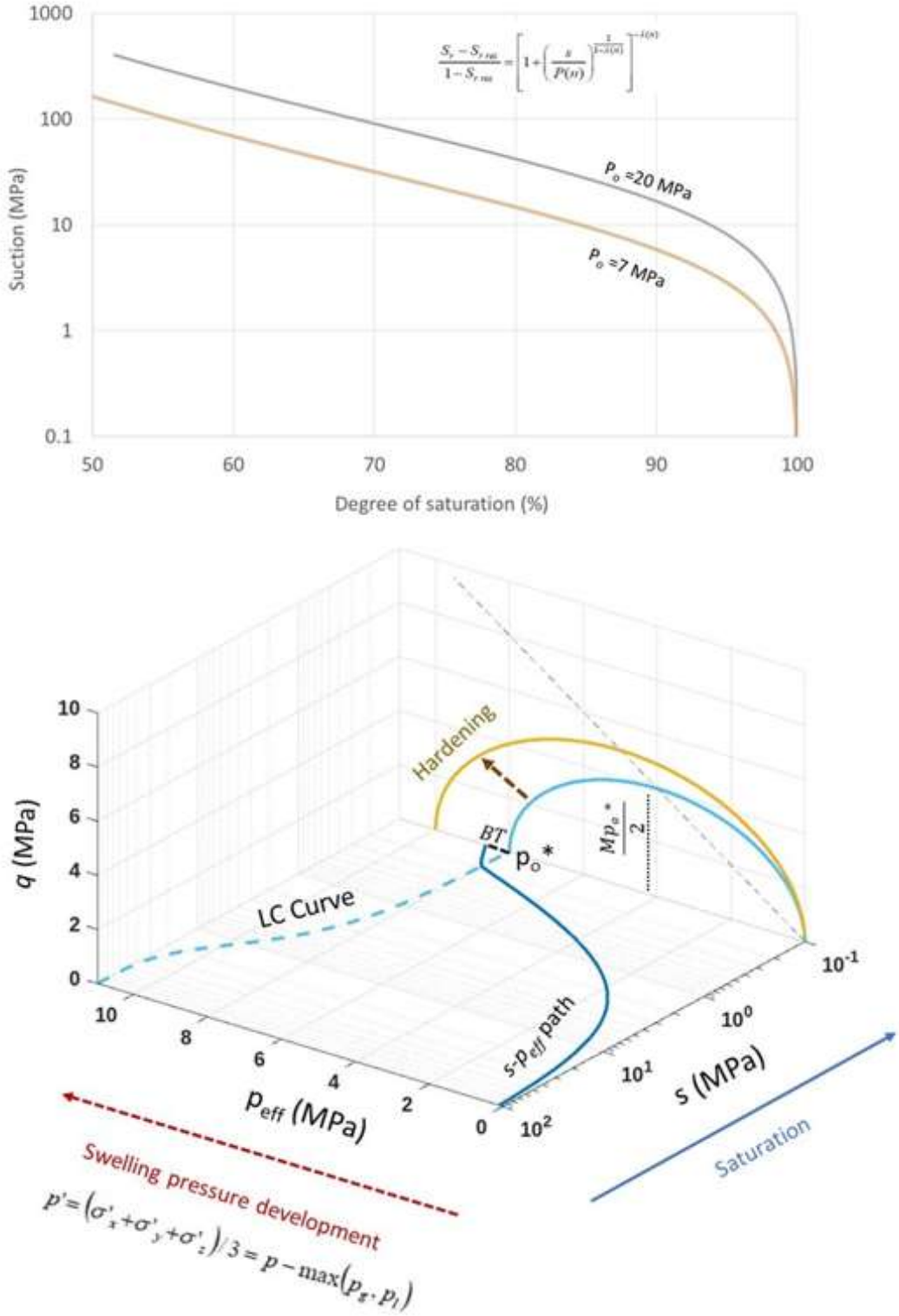

Figure 2.104: Water retention curve (above) and calibration of mechanical parameters (BBM) of the clay. LC curve and p_{eff}-q-s path (below).

The injector system have been introduced to the model as a boundary condition. Prescribed gas pressure has been applied from one end of the sample in the model. Boundary conditions have been shown in Figure 2.106). The model calibration has been performed by means of comparison of back pressures.

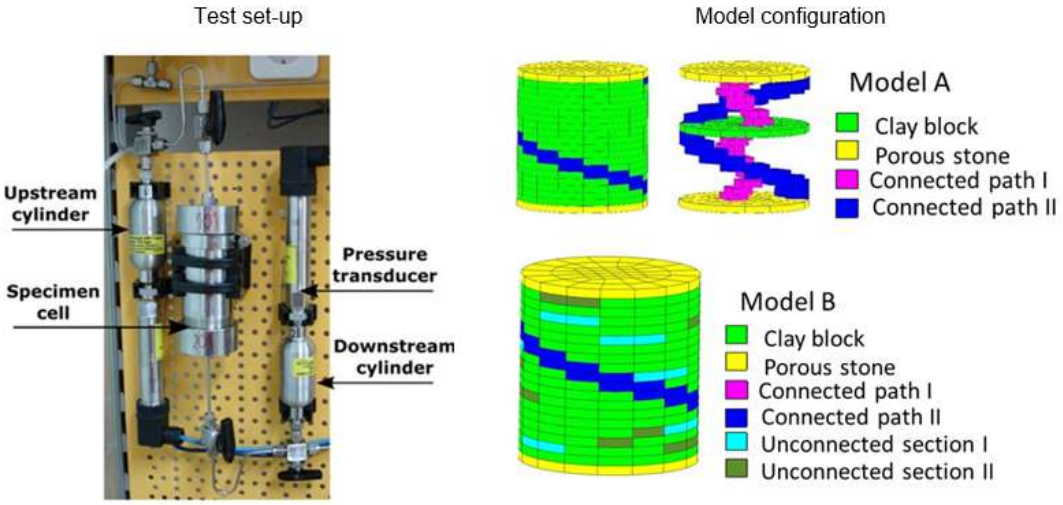

Figure 2.105: Test set-up and models (A and B) presentation (Gutiérrez Rodrigo, 2019). Model A and Model B correspond to arbitrary realization of heterogeneity assuming some preferential paths (A and B) and some random heterogeneous zones (B). In the future, more realizations should be done to analyse the response depending on the distribution of properties.

Hydraulic boundary conditions, together with time stepping and prescribed gas pressure on the upper and lower boundaries are depicted in Figure 2.106. The sample has been saturated during 60 days. After reaching the full saturation, gas injection takes place till breakthrough pressure. When the second breakthrough happens, the gas pressure source is closed. There is no water supply from lower or upper part of the sample during gas injection steps. There is no water or gas injection from lower part during gas injection steps. Lower part remains under initial conditions following to saturation (no gas or water injection).

Total inflow from upper boundary where the gas injection takes place and corresponding accumulated gas volume in the model are shown in Figure 2.107. At the end of first breakthrough, both in the test and in the model; total injected volume of gas is around 0.29 cm^3.

Hydro-mechanical parameters used for materials are listed in Table 2.26 and Table 2.27. Cubic law (Olivella and Alonso, 2008) has been used to simulate preferential paths as a permeability model (Figure 2.102 and Figure 2.103). The global intrinsic permeability is defined as sum of material matrix and internal fracture permeabilities. Cubic law parameters are calibrated by means of back-analyses. Barcelona Basic Model (BBM) (Alonso et al., 1990) has been used as the mechanical model for FEBEX. Porous stones are simulated as separate materials and have elastic parameters.

2.5.3. Model A

Figure 2.108 shows distribution of preferential paths in Model A. Two connected pathways have been incorporated to the geometry in a random manner. Model A corresponds to arbitrary realization of heterogeneity assuming some preferential paths. In the future, more realizations should be done to analyse the response depending on the distribution of properties.

Comparison of back pressure data and Model A results during Phase 2 and Phase 4 is summarised in Table 2.26. In Phase 4, a bigger back pressure has been succeeded. Figure 2.109 shows gas pressure development in the test (Phase 2 and Phase 4) and in the model. The response of back pressure in the Model A is similar to Phase 4. In the numerical model, back pressure develops in a more gradual way

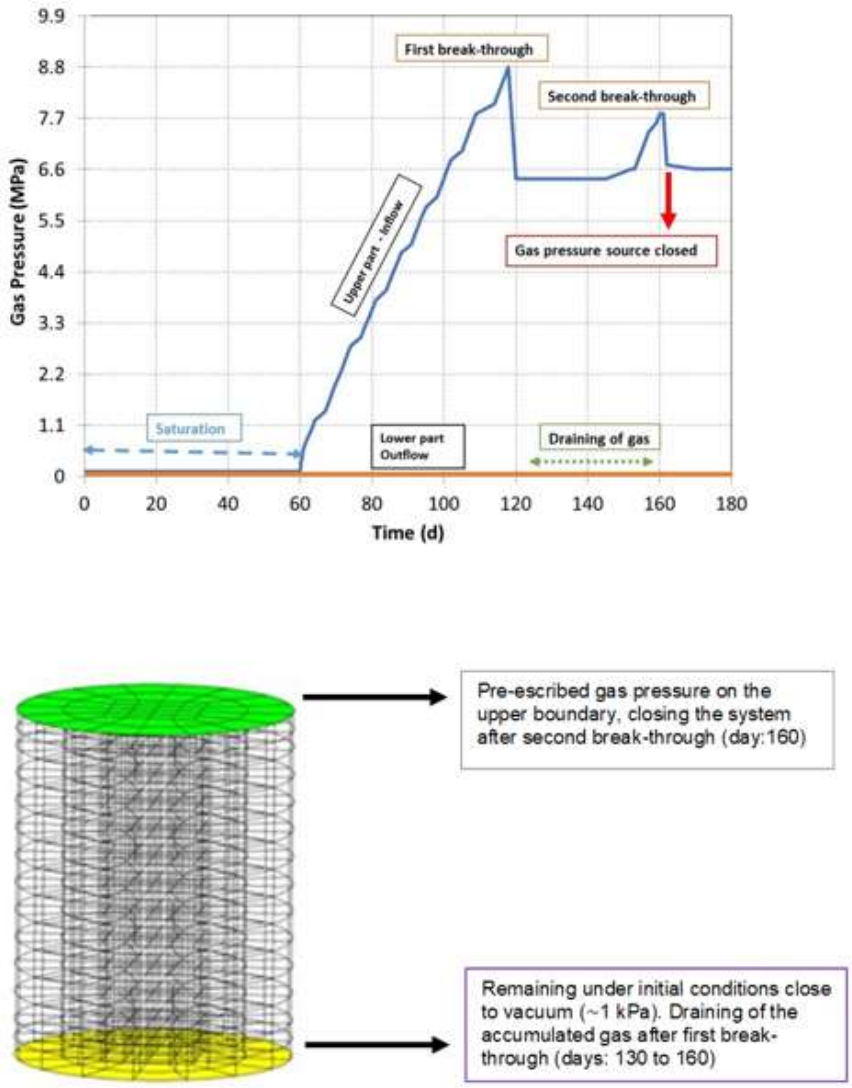

Figure 2.106: Gas pressure on the boundaries during gas injection steps.

compare to the test.

Figure 2.110 shows gas pressure distributions in 30, 58 (first BT), 90 (second BT) and 137 days later the gas injection initiation. Gas pressure evolution on the upper and lower part of the sample is also shown in Figure 2.110. First BT has occurred on 8.6 MPa and 4.4 MPa of back pressure has been achieved. Second BT has occurred in 7.6 MPa and 3.3 MPa of back pressure has been succeeded.

Figure 2.111 shows distribution of gas diffusion and gas advective flux in 30, 58 (first BT), 90 (second BT) and 137 days later the gas injection initiation. Gas advective fluxes through preferential pathways can be clearly seen during second BT (90 days).

Figure 2.112 shows mean total stresses distributions in 30, 58 (first BT), 90 (second BT) and 137 days later the gas injection initiation. In the Figure 2.112, mean total stress evolution in upper part of the sample is also shown. FEBEX bentonite was initially unsaturated. During the saturation period, swelling pressures have been developed. The total pressure reaches 8.9 MPa at the end of saturation process. After the saturation, water has been drained from the filters and gas injection test has re-started. Mean total stresses has reached to 8.6 MPa at the end of first BT. After first BT, residual gas has been drained from lower

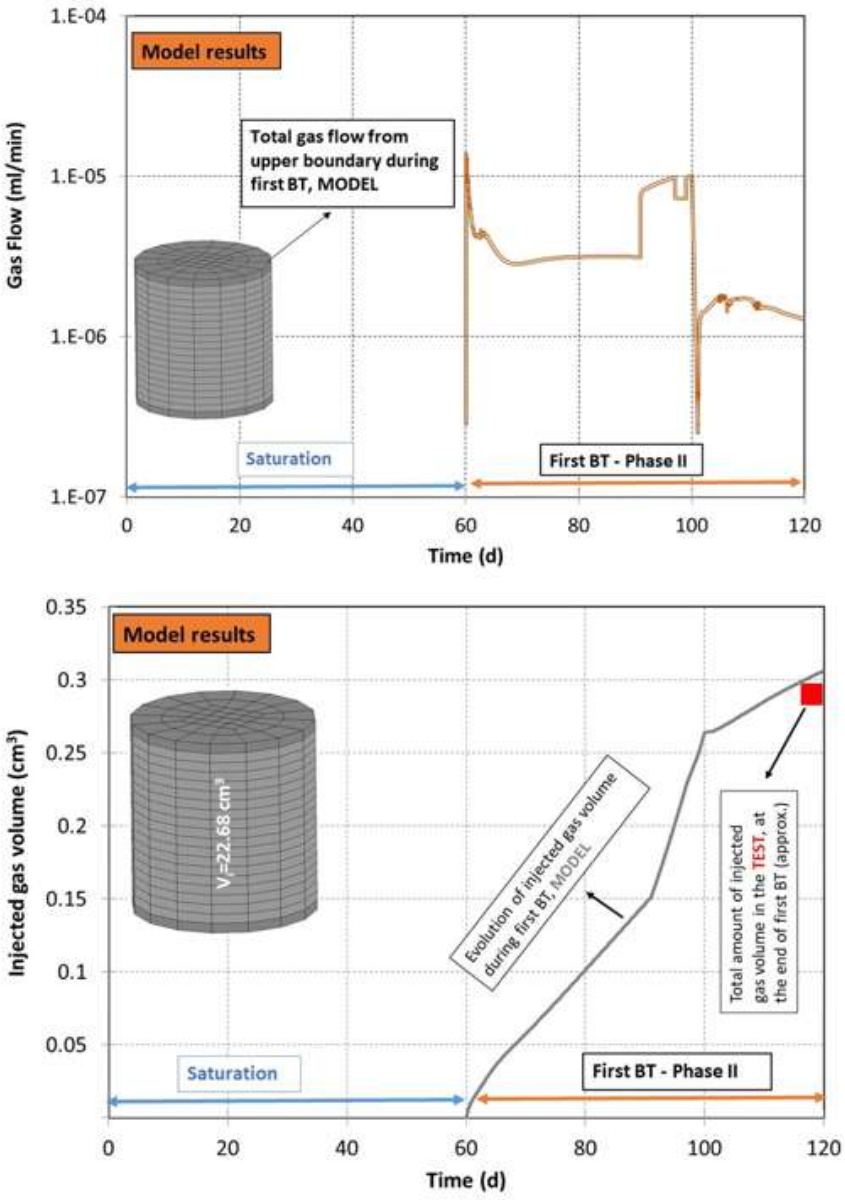

Figure 2.107: Total gas flow from upper boundary and corresponding accumulated injected gas volume in the Model A and in the Test.

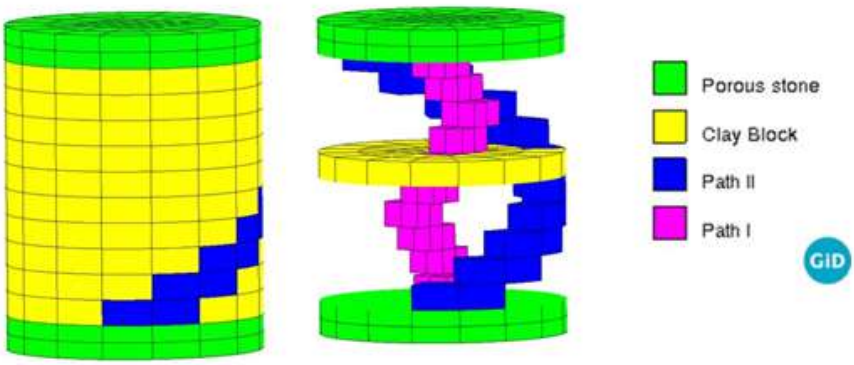

Figure 2.108: Materials considered in the model (A).

part of the sample and finally second BT test has started. The model is capable to simulate swelling pressure development during hydration; gas pressure development during gas injection test including draining process of water and gas under the same 3D configuration.

Table 2.26: Comparison of back pressure data and model results (Model A).

Breakthrough sequence	Back pressure (MPa)		
	Phase II	Phase IV	Model A
First BT	2.2	3.5	4.4
Second BT	1.7	3.4	3.3

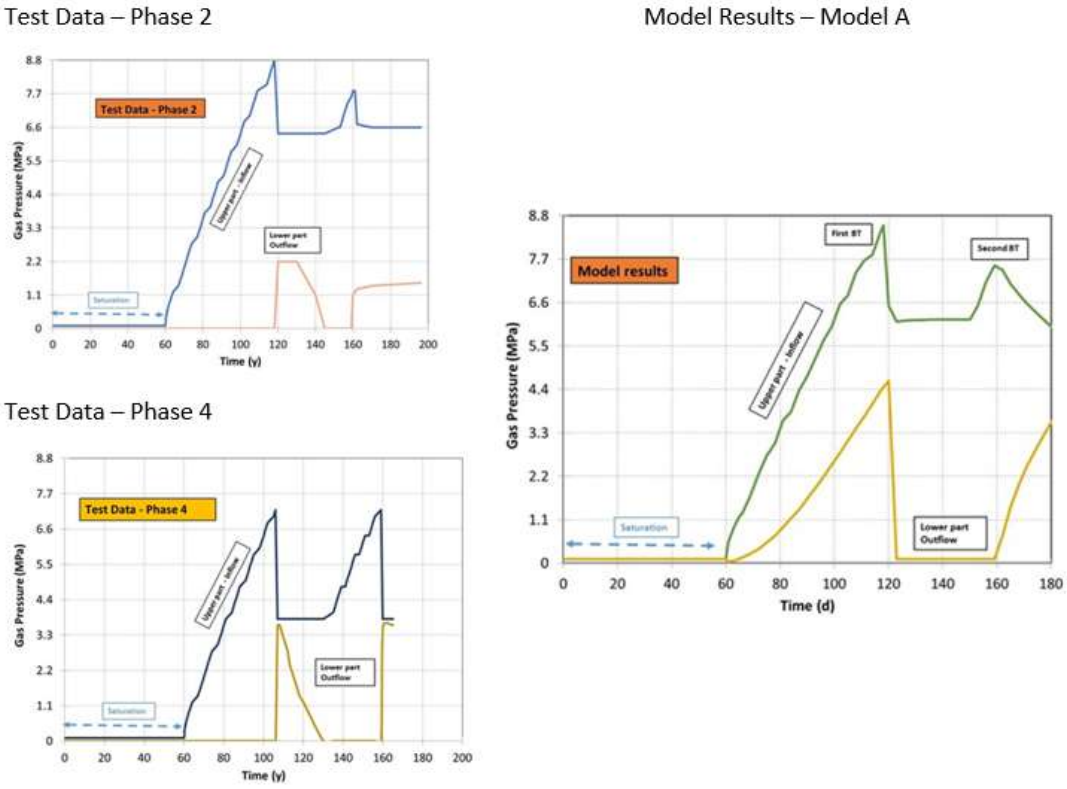

Figure 2.109: Gas pressure development in the tests and in the numerical simulation. (Model A)

2.5.4. Model B

Model B has been generated by means of incorporation of two unconnected sections into Model A geometry. Unconnected section I and unconnected section II has the same parameter set as Path I and Path II, respectively. As there are two unconnected sections in Model B, it is more heterogenous than Model A. Figure 2.113 shows distribution of connected paths and unconnected sections in Model B.

Model A and Model B correspond to arbitrary realizations of heterogeneity assuming some preferential paths (A and B) and some random heterogeneous zones (B). In the future, more realizations should be done to analyse the response depending on the distribution of properties.

Figure 2.114 shows gas pressure development in the test (Phase 2 and Phase 4) and in the Model B. Response of back pressure in the Model B is similar to Phase 4. In the numerical model, back pressure develops in a more gradual way compare to the test.

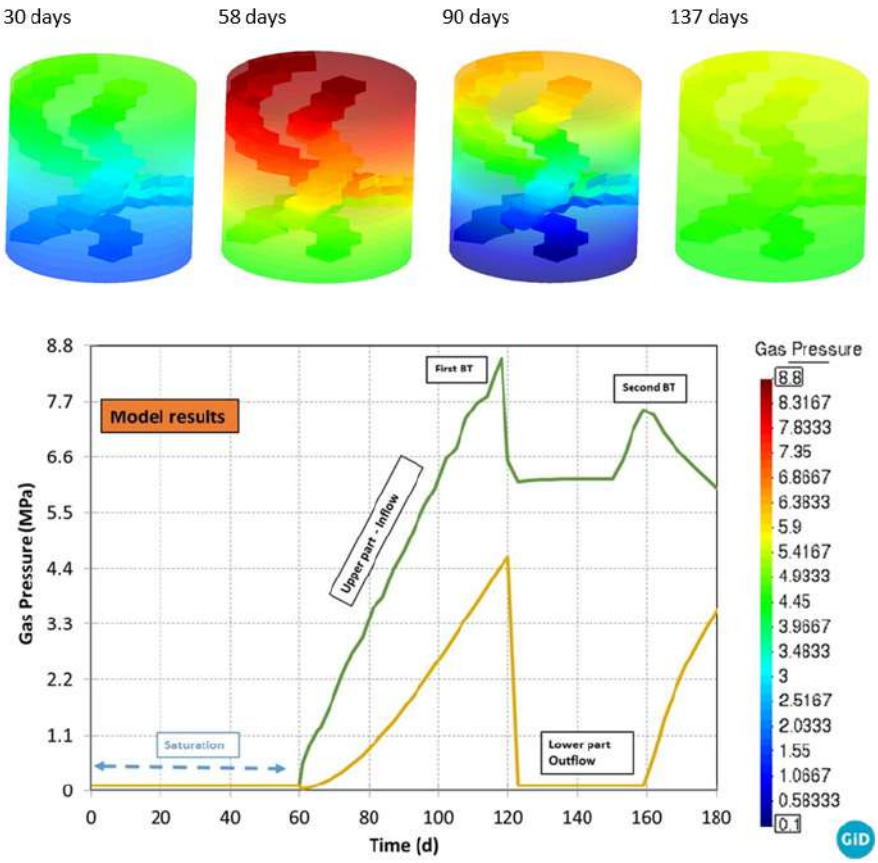

Figure 2.110: Gas pressure distributions in 30, 58 (first BT), 90 (second BT) and 137 days later the gas injection initiation. Gas pressure evolution on the upper and lower part of the sample. (Model A)

Figure 2.115 shows permeability evolution on the upper parts of the sections and distribution (during second BT) in Model B. As the pathways and unconnected sections have cubic law, intrinsic permeability increases during the aperture of these pathways. After the first breakthrough, intrinsic permeability of pathways stabilizes. Once the gas injection re-starts (second BT), pathways are activated and intrinsic permeability starts increasing again. After second BT, gas injection stops and intrinsic permeability of pathways decreases because of closure of fractures.

Figure 2.116 shows distribution of gas advective fluxes in 15, 30, 45 and 60 days in Model B. Gas advective fluxes have been concentrated on preferential pathways. Figure 2.117 shows comparison of gas diffusion (plus gas dispersion), gas advection and gas pressure at 60 days later injection. Diffusion is active in all model domain because it is non advective flux and there is no need of apertures and/or desaturation for gas diffusion. Additionally, gas diffusion is more dominant where gas advection is less relevant. Gas advection shows the preferential path formation.

2.5.5. Extended Models A and B

Model A_Extended and Model B_Extended correspond to time prolonged models that simulate all phases of the test. A summary of the phases and comparison of time stepping of the models are given in Table 2.27. After Phase II, the sample was dismantled and re-saturated. Following to re-saturation, gas injection was performed till first BT in Phase IV. The first BT pressure in Phase IV was 7.1 MPa resulting 3.5 MPa of back pressure. The second BT pressure in Phase IV was 6.6 MPa resulting 3.4 MPa of back pressure. compared to Phase II, gas BT pressures are lower but back pressures are higher. Mean value of gas BT pressure for the whole processes is 7.6 MPa and back pressure is around 3 MPa. There are differences

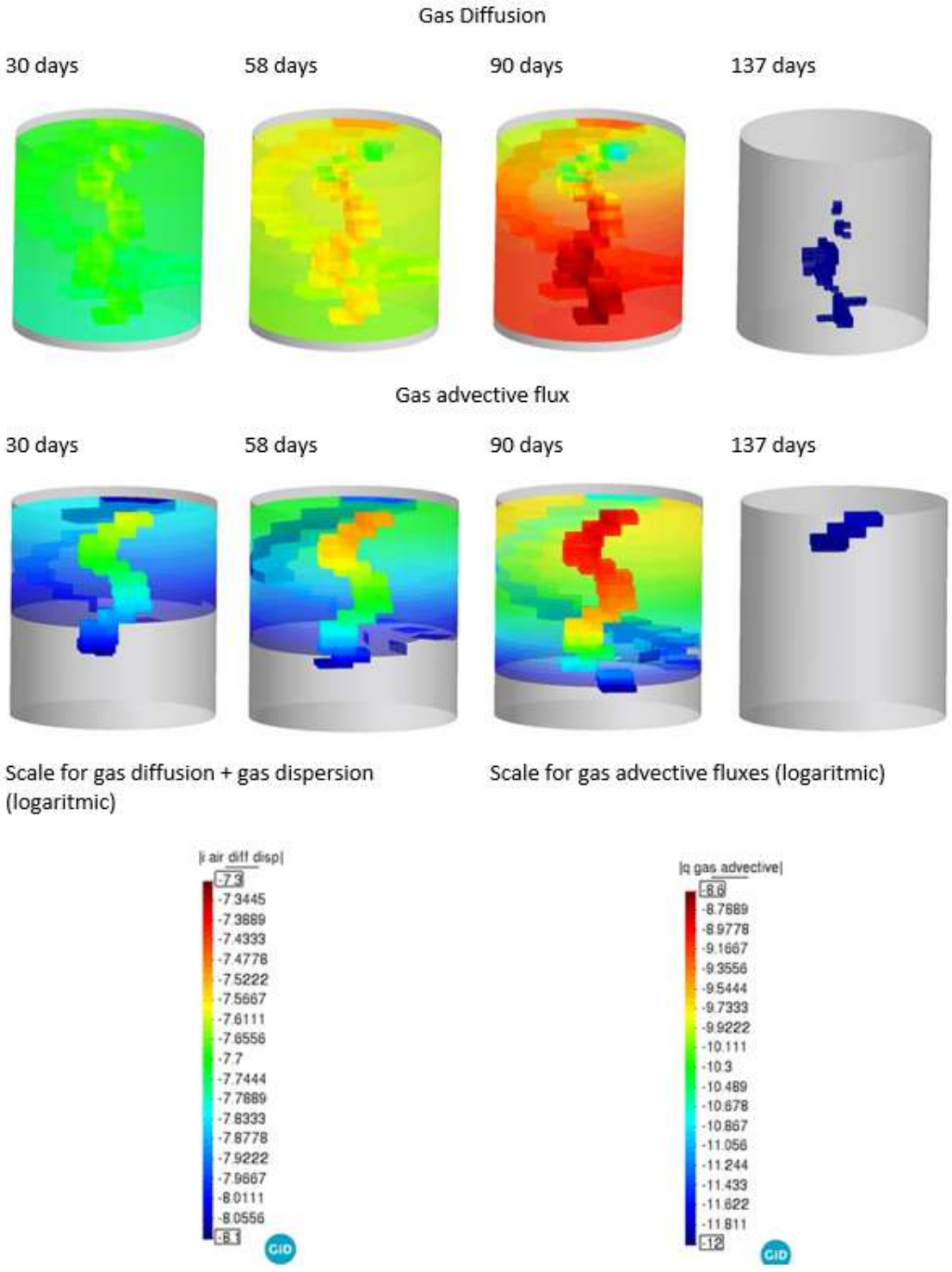

Figure 2.111: Distribution of gas diffusion and gas advective flux in 30, 58 (first BT), 90 (second BT) and 137 days later the gas injection initiation. (Model A)

between Phase II and Phase IV in terms of gas BT and back pressures because of changes in porosity-permeability and material structure during the whole process.

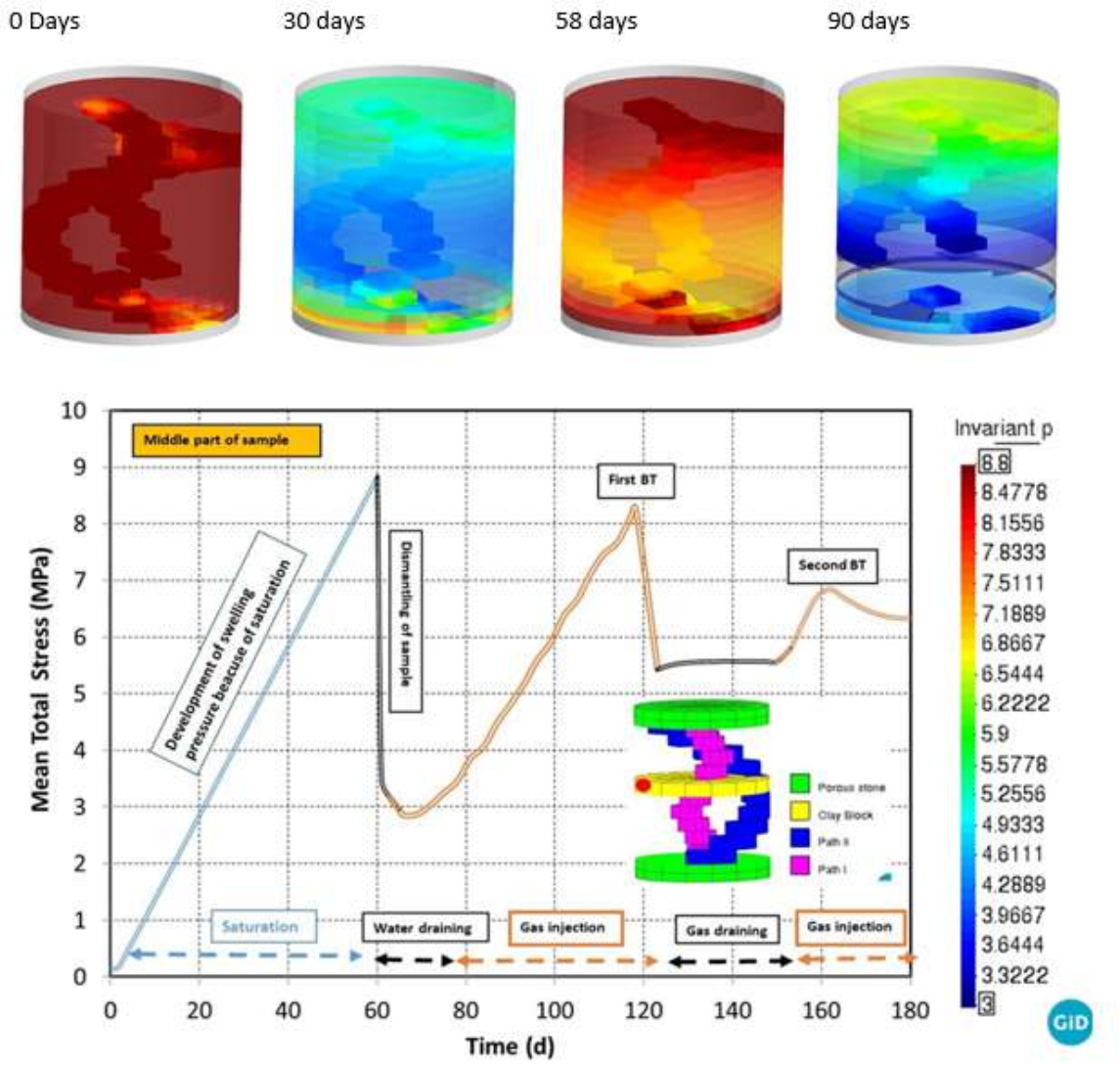

Figure 2.112: Mean total stresses distributions in 30,58 (first BT), 90 (second BT) and 137 days later the gas injection initiation. Mean total stress evolution on the middle part of the sample. (Model A)

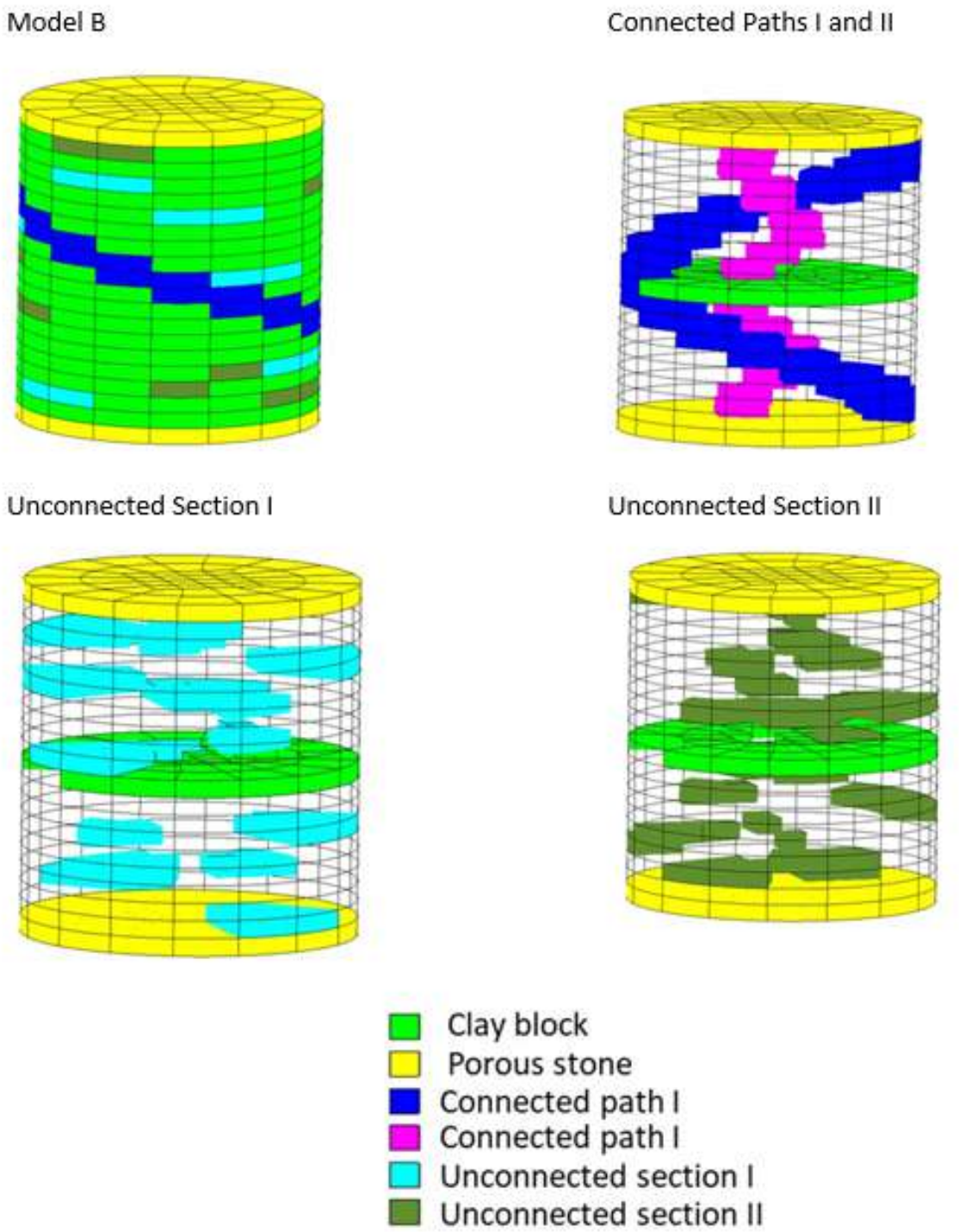

Figure 2.113: Distribution of materials in Model A.

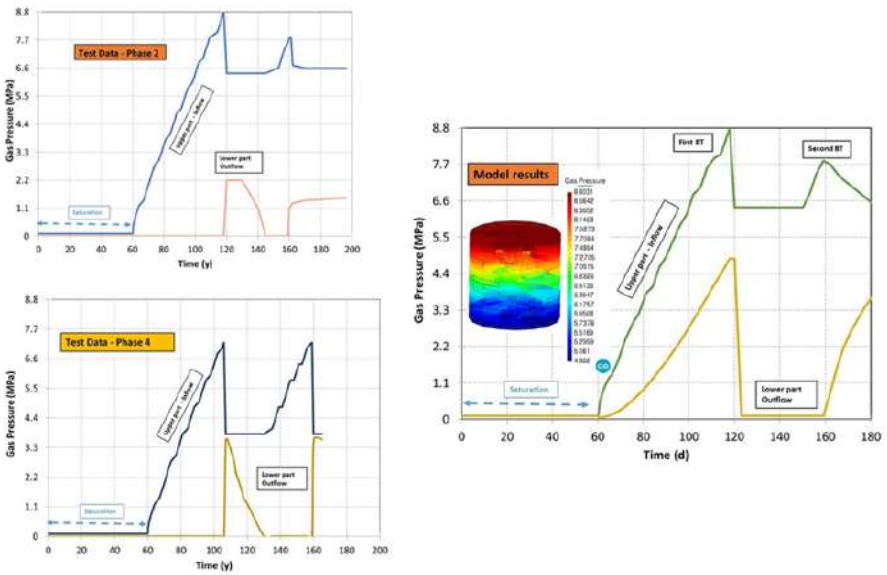

Figure 2.114: Gas pressure development in the tests and in the numerical simulation. (Model B)

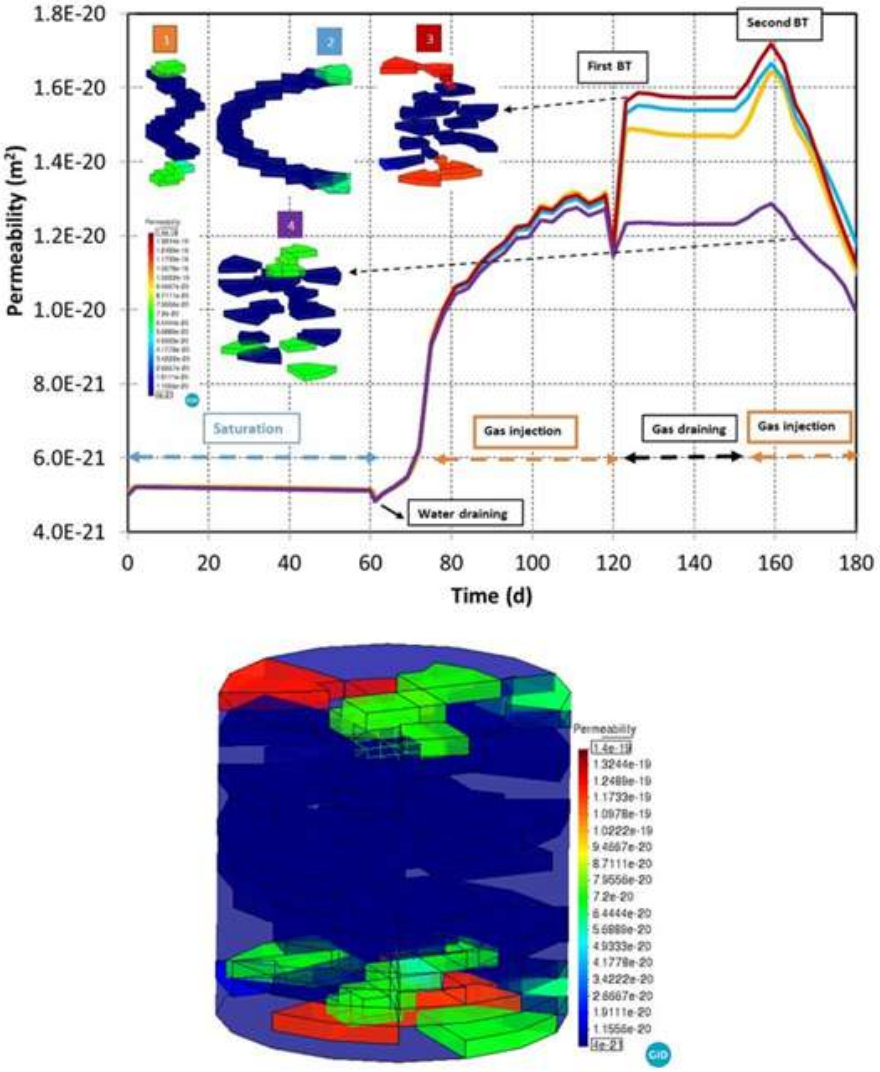

Figure 2.115: Permeability evolution on upper part of the sections and distribution (during second BT) for Model B.

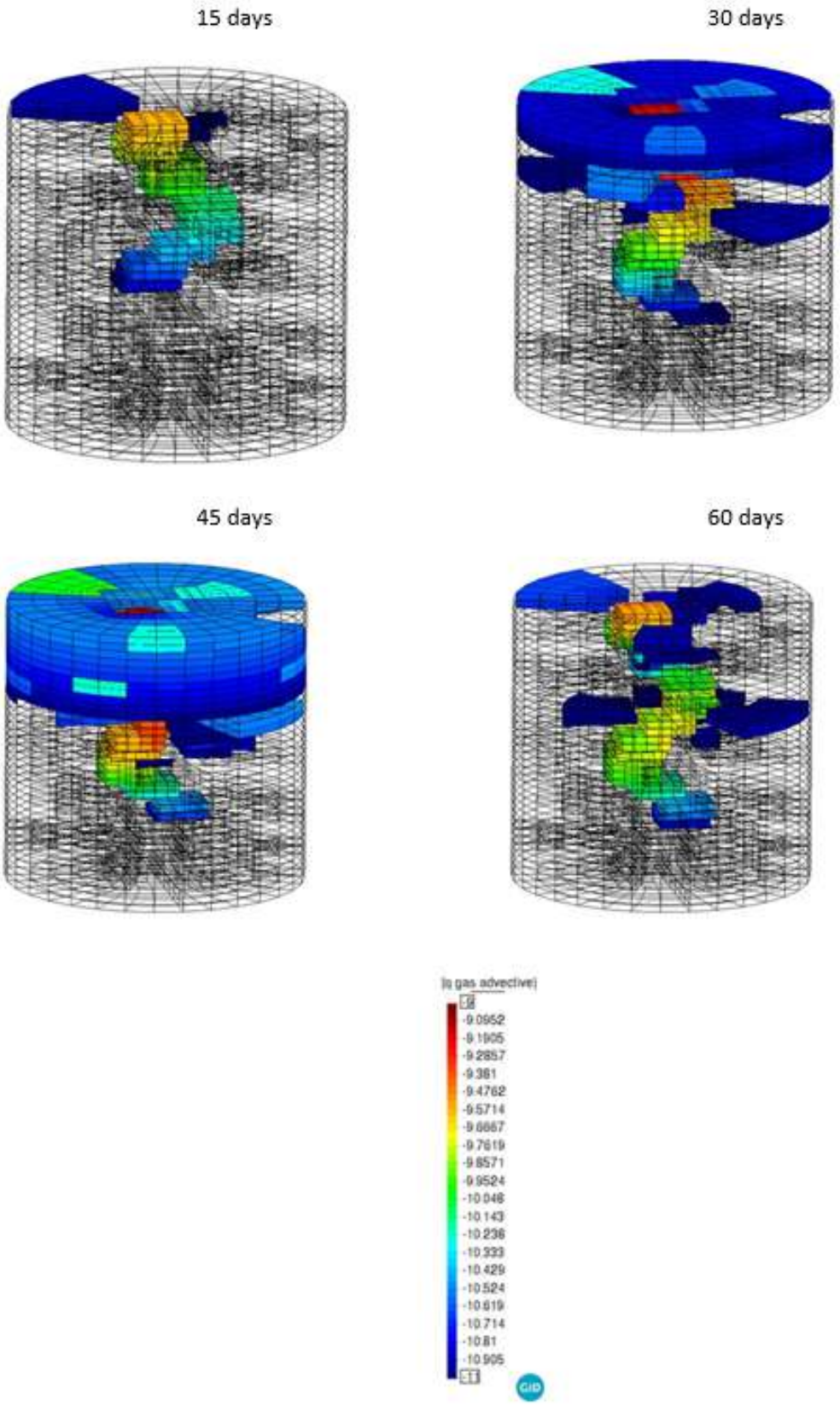

Figure 2.116: Distribution of gas advective fluxes (logarithmic scale) at 15, 30, 45 and 60 days for Model B.

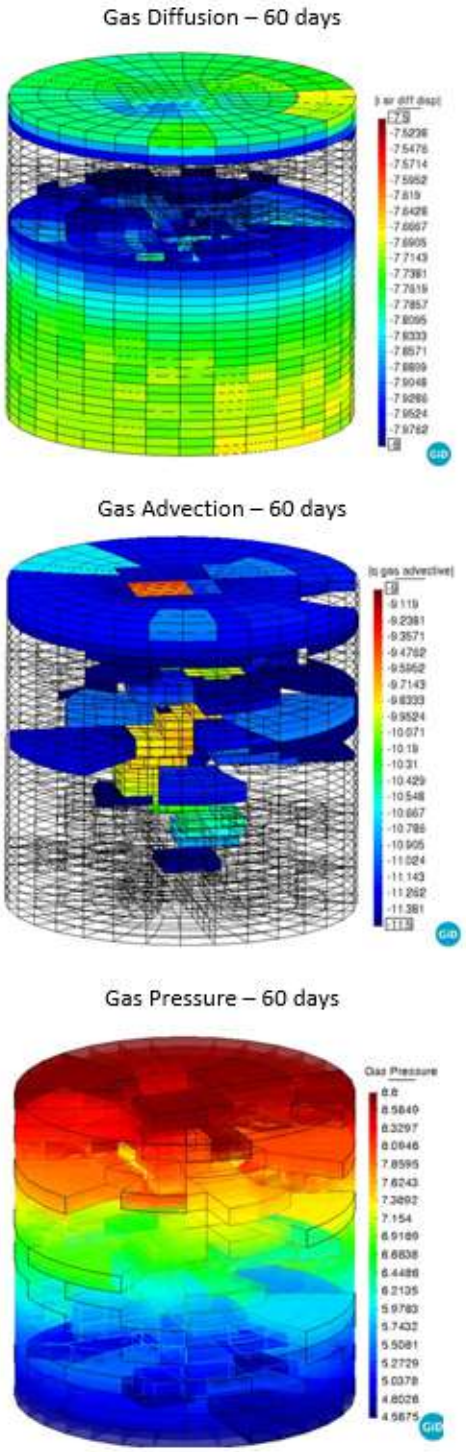

Figure 2.117: Distribution of gas diffusion (plus dispersion), gas advection and gas pressure at 60 days (Model B).

Table 2.27: Comparison of Model A, Model B and Model A_Extended.

Steps of breakthrough tests	Description	Duration (d)	Model A Model B	Model A_Extended Model B_Extended
Phase I	Saturation of the sample	60	+	+
Phase II	Gas injection - first breakthrough pressure	60	+	+
	Gas injection - second breakthrough pressure	80	+	+
Phase III	Dismantling of the sample and re-saturation	60	-	+
Phase IV	Gas injection - first breakthrough pressure	50	-	+
	Gas injection - second breakthrough pressure	50	-	+

Comparison of back pressures in the test and in the models are summarized in **Table 2.28**. Models prediction of back pressures at Phase IV is better than Phase II.

Table 2.28: Comparison of back pressure data and model results (Model A_Extended and Model B_Extended).

Breakthrough sequence	Back pressure (MPa) Test		Model A_Extended		Model B_Extended	
	Phase II	Phase IV	Phase II	Phase IV	Phase II	Phase IV
First BT	2.2	3.5	4.5	3.5	4.5	3.6
Second BT	1.7	3.4	4.5	3	4.6	3

Figure 2.118 shows gas pressure distributions in 120 (Phase II - first BT), 160 (Phase II - second BT), 310 (Phase IV - first BT) and 365 days (Phase IV - second BT). Gas pressure evolution on the upper and lower part of the model domain is also shown in Figure 2.118. In Model A_Extended and in Model B_Extended, back pressure value in Phase IV (first BT) is around 3.5 MPa which is consistent with the test data. Model A_Extended slightly overestimates back pressure in Phase II.

Figure 2.119 and Figure 2.120 shows evolution of total mass fluxes. There are three gas fluxes in the system which are gas advective fluxes (acting on preferential pathways and causing de-saturation because of water replaced by gas), dissolved advective fluxes (flux of dissolved gas into liquid phase) and non-advective fluxes (gas diffusion + dispersion). The sum of these three fluxes gives the total mass fluxes. As shown in Figure 2.119 and Figure 2.120, on the upper part where gas injection takes place; the dominant flux is gas advective flux. However, in central area of the model domain gas diffusion (dissolved non-advective flux) is more significant.

2.5.6. Sensitivity Analyses

In this Chapter, sensitivity analyses are described. The aim of the sensitivity analyses is to improve model capabilities and deal with the data uncertainties. Sensitivity analyses represent alternative material models, geomechanic model parameters and/or initial and boundary conditions. Sensitivity analyses shall remain within the scope set for the reference model in order to maintain modelling consistency. In this

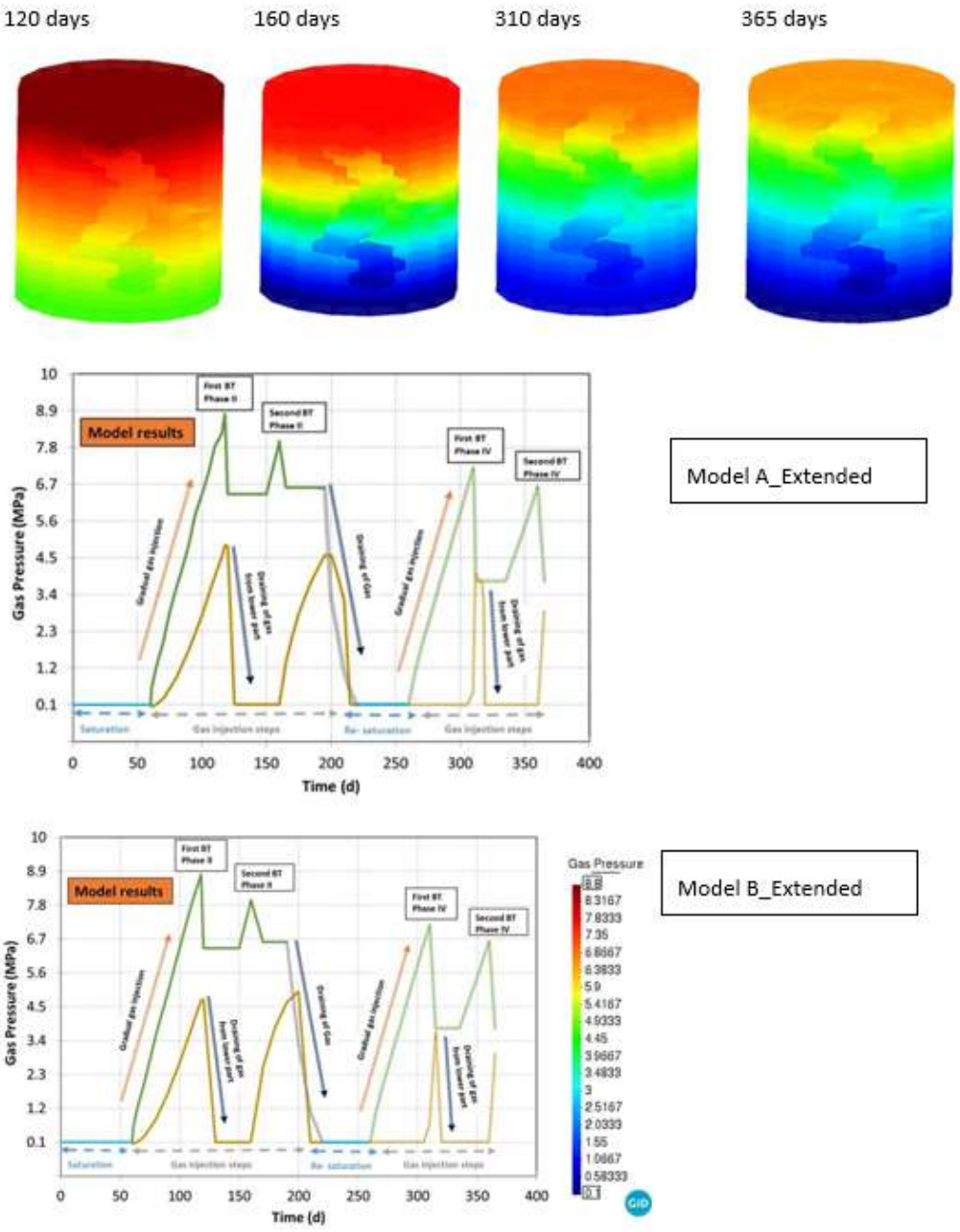

Figure 2.118: Gas pressure distributions in 120 (Phase II - first BT), 160 (Phase II - second BT) and 310 (Phase IV - first BT), 365 (Phase IV - second BT). Gas pressure evolution upper and lower part of the sample (Model A_Extended and Model B_Extended).

study, Model A has been selected as a reference model in order to develop further sensitivity analyses. Beside Model A_Extended, two more models have been prepared in order to check impact of time step (adding more phases of the test), number of nodes-elements and hydro-mechanical model parameters (gas relative permeability parameters, water retention curve parameters, pressure of pre-consolidation and heterogeneous porosity distribution) on the model response. These models are summarized in Table 2.29.

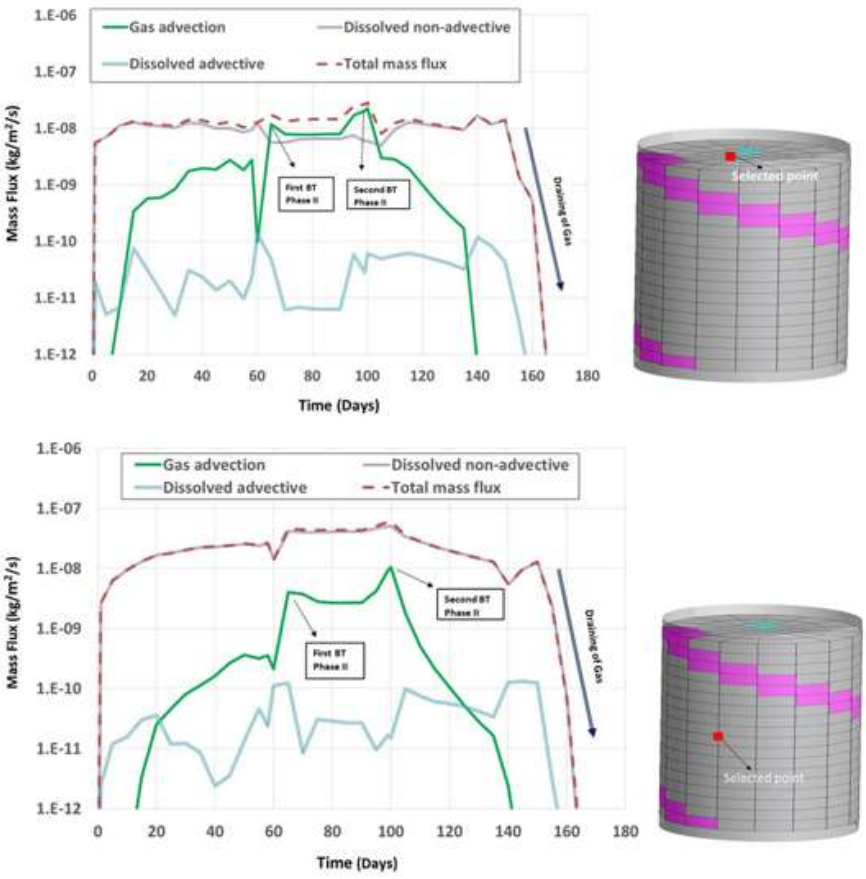

Figure 2.119: Evolution of mass fluxes till Phase III at selected points for Model A_Extended.

Table 2.29: Sensitivity analyses plan

Concept	Observation	Model
Time step	Phase III (re-saturation) and Phase IV (secondary gas injection steps) have been incorporated to Model A.	Model A_Extended (described in Chapter 2)
Hydro-mechanic	Initial heterogenous distribution of porosity has been incorporated to Model A.	Model A_Extended_1
Hydraulic	Gas relative permeability parameters have been modified. Total gas permeability has been increased. Gas entry pressure has been decreased. P_0 (WRC) has been decreased to 7 MPa from 20 MPa. (Figure 2.104, Chapter 1).	Model A_Extended_2
Mechanic	Pressure of pre-consolidation of the clay has been decreased to 8 MPa from 12 MPa (Figure 2.104, Chapter 1). Plasticity has been targeted as the Gas BT pressure was 8.8 MPa.	Model A_Extended_2

Table 2.29: Sensitivity analyses plan

Concept	Observation	Model
Computational	Number of nodes and elements have been increased in order to simulate better heterogeneity of the system.	Model A_Extended_1

Model A_Extended is a prolongation of Model A under the same geometrical configuration (connected paths). Phase III (dismantling of the sample and re-saturation) followed by Phase IV (gas injection steps) have been incorporated to Model A_Extended as discussed in Chapter 2. Figure 2.121 shows initial porosity distribution and describes main differences between the models.

Distribution of gas advective fluxes during the first BT (58 days later gas injection) are shown in Figure 2.122. Gas advective fluxes are mainly concentrated on preferential pathways. Permeability increases on these paths during gas injection because of apertures (cubic law for permeability). In Model A_Extended_2, gas permeability is the highest. Therefore, gas advection flux is the biggest in this model.

Distribution of gas diffusion (plus dispersion) during the first BT (58 days later gas injection) are shown in Figure 2.123. Gas diffusion is less relevant where the gas advection is more significant. While gas advection fluxes are mainly intensified on preferential pathways, gas diffusion is active in whole domain. For the gas diffusion there is no need of neither desaturation nor gas flow pathways development. Gas diffusion is mainly controlled by the porosity.

In Model A_Extended_1, initial distribution of porosity is heterogeneous. Consequently, distribution of gas advection fluxes and gas diffusion is relatively more heterogeneous in Model A_Extended_1 compare to other two models.

Figure 2.124 and Figure 2.125 shows evolution of total mass fluxes. There are three fluxes in the system which are gas advective fluxes, dissolved advective fluxes (dissolved gas into liquid phase) and non-advective fluxes (diffusion + dispersion). The sum of these three fluxes gives total mass fluxes as discussed in Chapter 2.

A node close to gas injection source has been selected in order to compare total fluxes in these three models. Gas advection is dominant in this selected point. Gas advection is more active in Model A_Extended_2 compare to other models because of higher gas permeability. As shown in Figure 2.125, total mass fluxes are bigger in Model A_Extended_2. There is no significant differences between Model A_Extended and Model A_Extended_1 during the first and second BT in terms of total mass fluxes. In the model, prescribed gas pressure has been applied from the upper part of the model domain. In three models, the prescribed pressures are same. However, there have been more total gas fluxes in Model A_Extended_2 because of higher permeability (both liquid and gas) and lower gas entry pressure.

Distribution of permeability during the first BT (58 days later gas injection) for three models are shown in Figure 2.126. In the preferential pathways, the permeability is higher compare to other sections in all three models. Model A_Extended_2 is more permeable than the other two models.

Distribution of liquid saturation degree during the first BT (58 days later gas injection) for three models are shown in Figure 2.127. Evolution of permeability and degree of saturation are shown in Figure 2.128. The sample was initially unsaturated. During the hydration period, it reaches the full saturation. Once the gas injection started, liquid replaced by the gas because of gas advective fluxes. Therefore, de-saturated zones

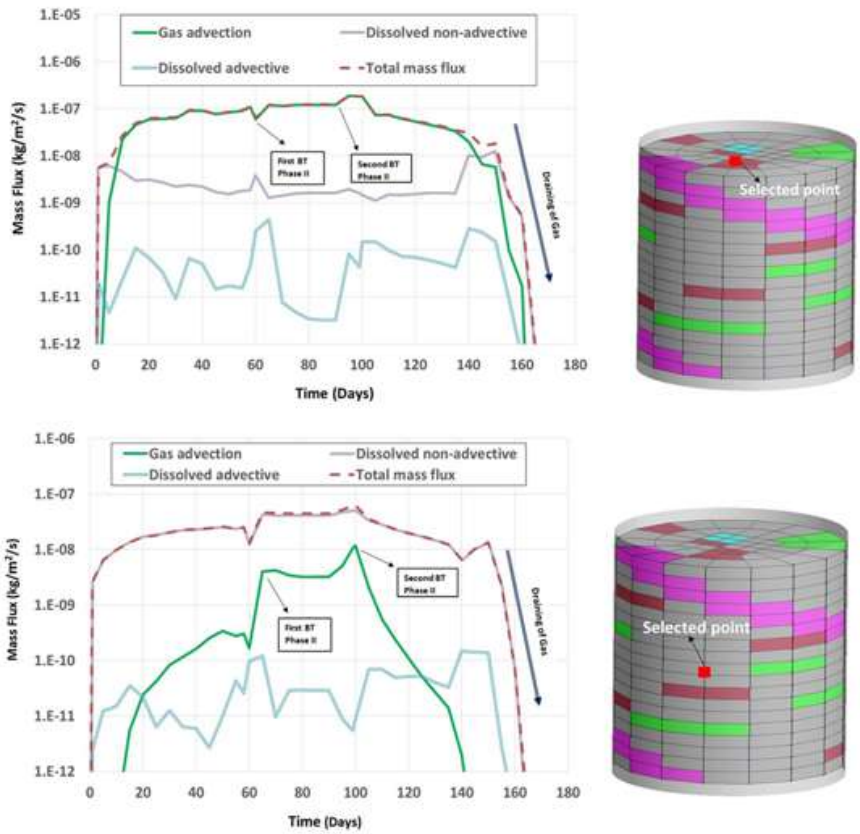

Figure 2.120: Evolution of mass fluxes till Phase III for Model B_Extended.

correspond to gas advective fluxes and show the preferential gas flow pathways. Similarly, permeability increases where the gas advective fluxes are significant. Hence both distribution of de-saturated zones and increased permeabilities indicate possible gas flow pathways.

Initial permeability (Figure 2.128) in Model A_Extended and Model A_Extended_1 is not same because of heterogenous distribution of porosity in Model A_Extended_1. In Model A_Extended_2, initial liquid permeability is one order bigger than the other two models. Permeability increases during gas injection and decreases during draining of gas in all three models.

Although Model A_Extended_2 is more permeable, it has a lower P_0 (water retention curve) value. Therefore, during gas breakthrough the de-saturation has been more significant (Figure 2.128) in Model A_Extended_2. However, re-saturation because of gas draining is faster in Model A_Extended_2 as it is more permeable.

Distribution of gas pressure during the first BT (58 days later gas injection) for three models are shown in Figure 2.129. Back pressures are around 4.6 MPa in Model A_Extended and Model A_Extended_1. Gas pressure distribution is relatively heterogeneous in Model A_Extended_1 because of initial heterogeneous distribution of porosity. In Model A_Extended_2, the highest back pressure has been succeeded as the total gas permeability was bigger in this model. The back pressure reaches to 8.4 MPa at the end of 58 days later gas injection initiation in Model A_Extended_2, which is significantly bigger than the test data.

Distribution of mean total stresses during the first BT (58 days later gas injection) for three models are shown in Figure 2.130. In Model A_Extended_2, the mean total stresses are bigger than the other two models at the end of 58 days of gas injection (first BT).

Evolution of gas pressure on the top (close to gas injection source) and the bottom (back pressure) to-

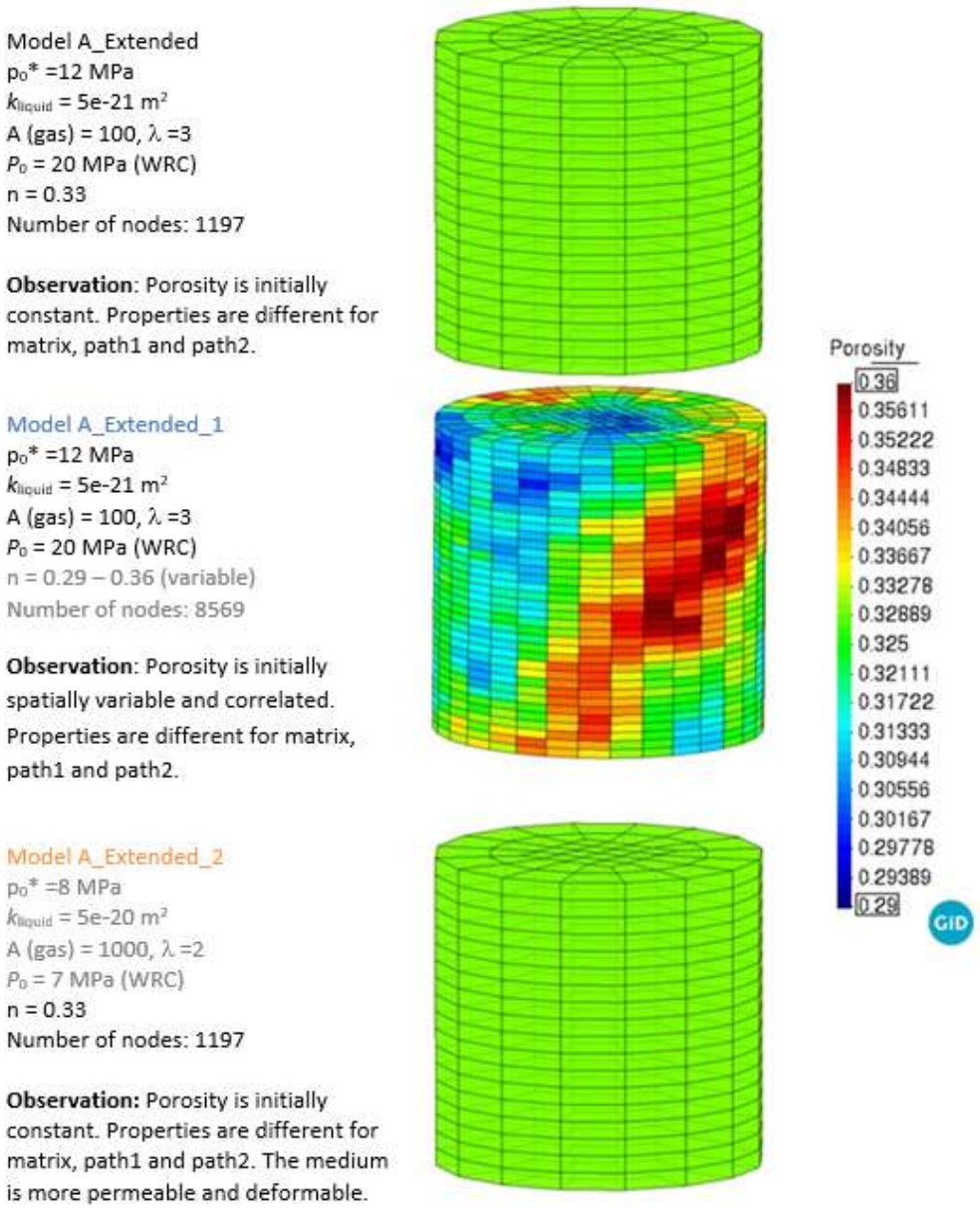

Figure 2.121: Distribution of initial porosity in three models.

gether with evolution of mean total stresses on central area are shown in Figure 2.131. In Phase II, back pressures were around 2.3 MPa and in Phase IV it was 3.5 MPa in the test. Model A_Extended and Model A_Extended_1 can predict adequately back pressures in Phase IV and slightly overestimate back pressures in Phase II. However, Model A_Extended_2 overestimates significantly back pressures in Phase II as it has a bigger permeability and lower gas entry pressure compare to other two models.

As shown Figure 2.131, developed mean total stresses during hydration (swelling pressure plus liquid pressure) in Model A_Extended_2 are lower compare to other two models. As preconsolidation pressure is lower in Model A_Extended_2, there has been less swelling pressure development during saturation phase. However, mean total stresses in Model A_Extended_2 are higher compare to other models during gas injection. As Model A_Extended_2 is more permeable, there is more gas pressure development on the selected point (central area) leading to higher mean total stresses. During the gas withdrawal from the lower part (draining of gas), the pressure dissipation is more significant in Model A_Extended_2 compare to other two models as it is more permeable.

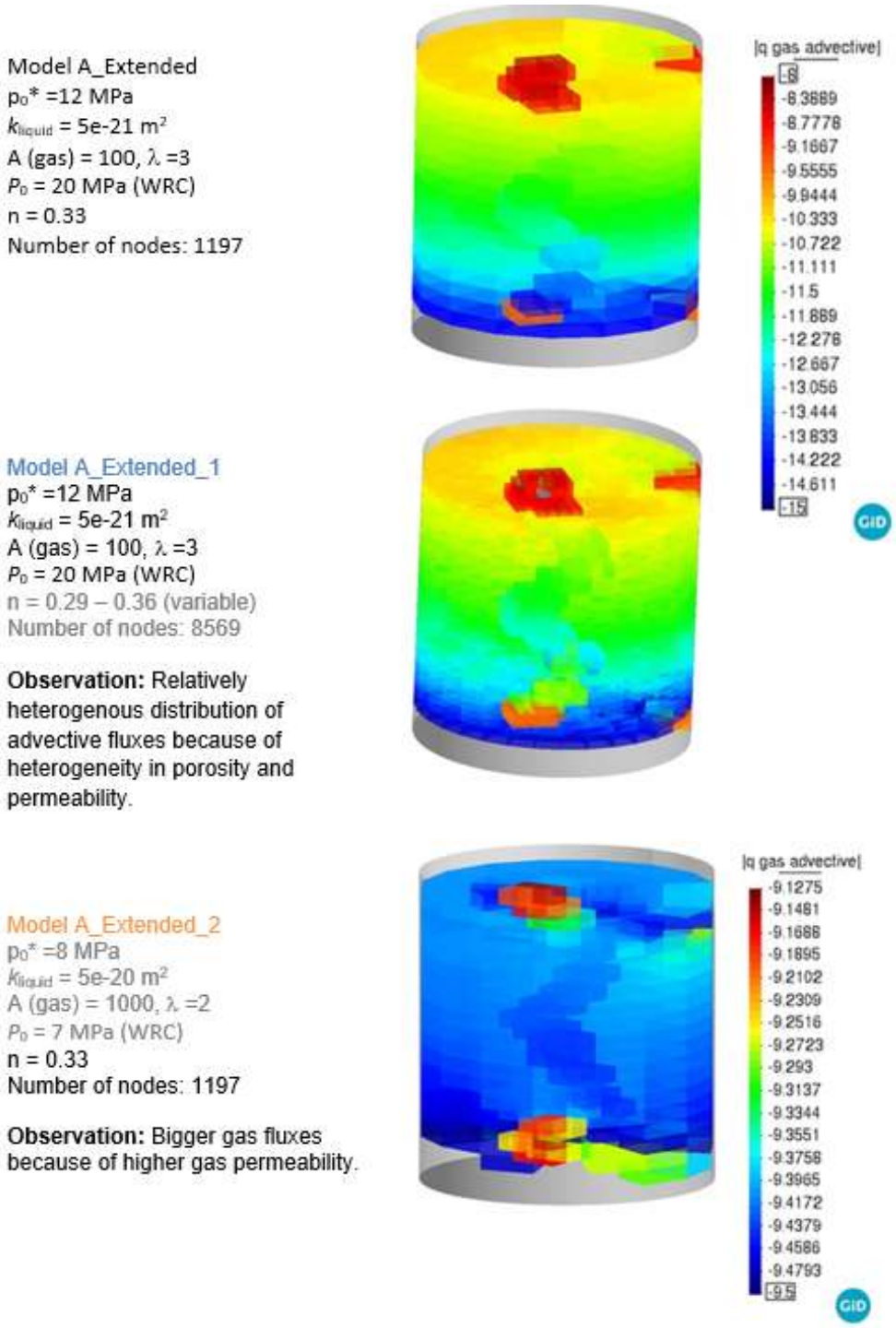

Figure 2.122: Distribution of gas advective fluxes (logarithmic scale) in three models during first breakthrough (58 days later gas injection).

Distribution of preconsolidation pressures during the first BT (58 days later gas injection) for three models are shown in Figure 2.132. In Model A_Extended_2, preconsolidation pressure has been considered as 8 MPa which is lower than the maximum gas BT pressure (8.8 MPa). Therefore, plasticity has been observed in this model. In Model A_Extended and Model A_Extended_1 preconsolidation pressure has been set as 12 MPa. Therefore, these two models are in elastic regime.

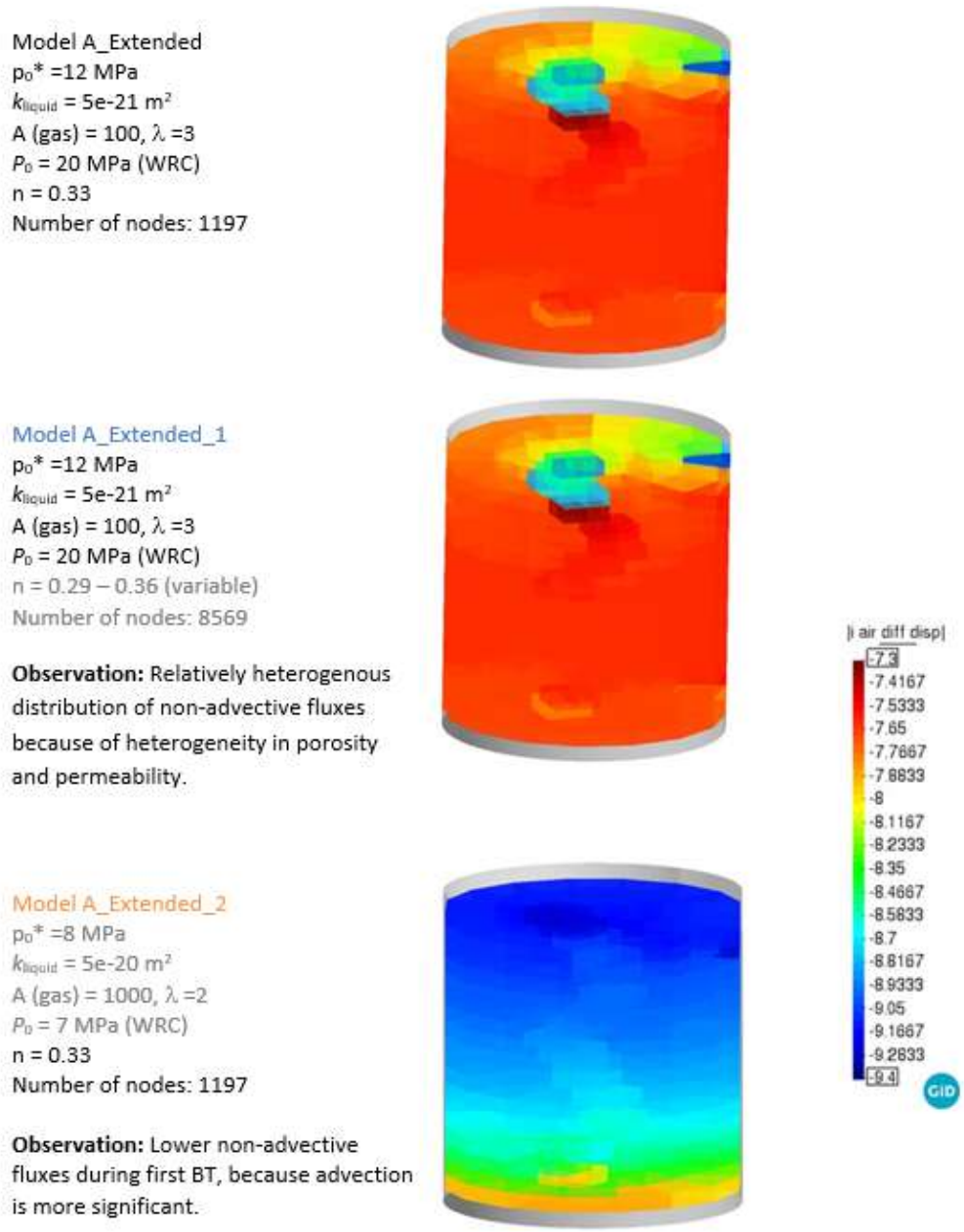

Figure 2.123: Distribution of gas diffusion plus dispersion (logarithmic scale) in three models during first breakthrough (58 days later gas injection).

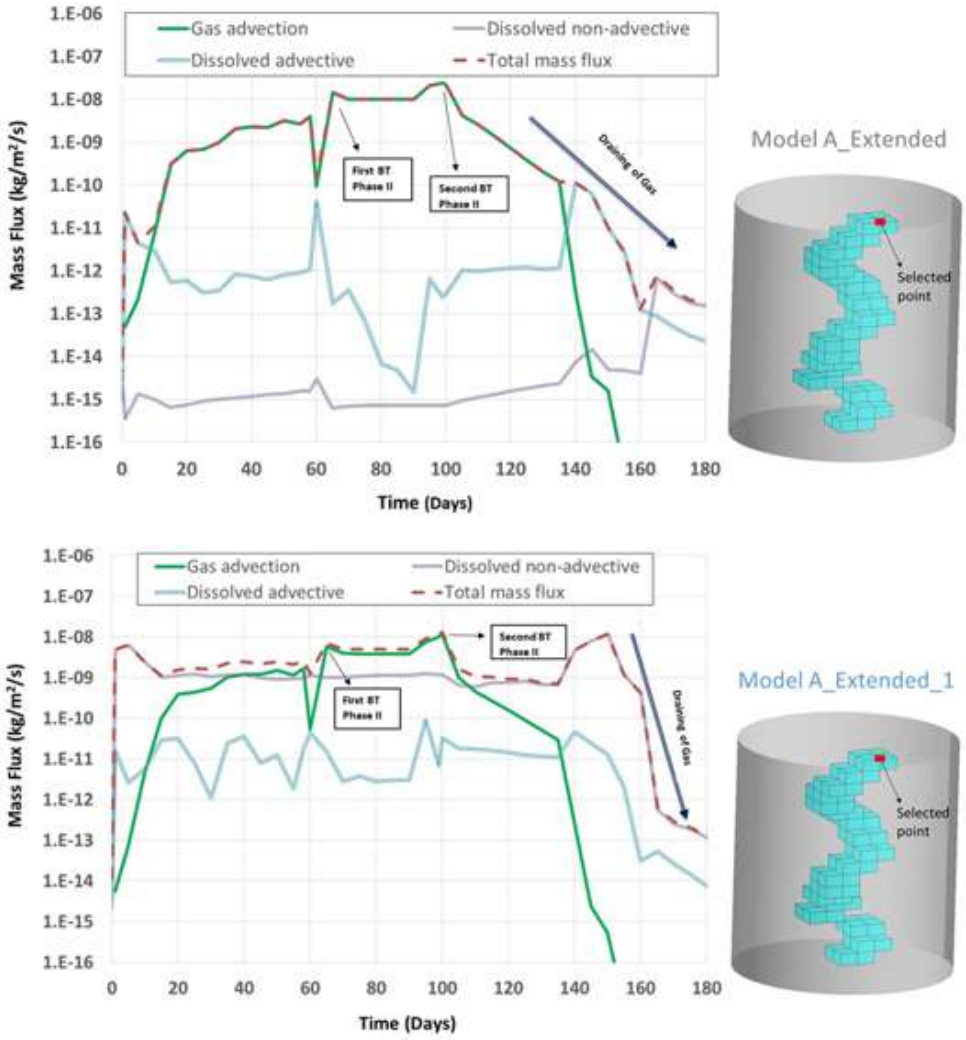

Figure 2.124: Mass fluxes at selected points in Model A_Extended (above) and Model A_Extended_1 (below).

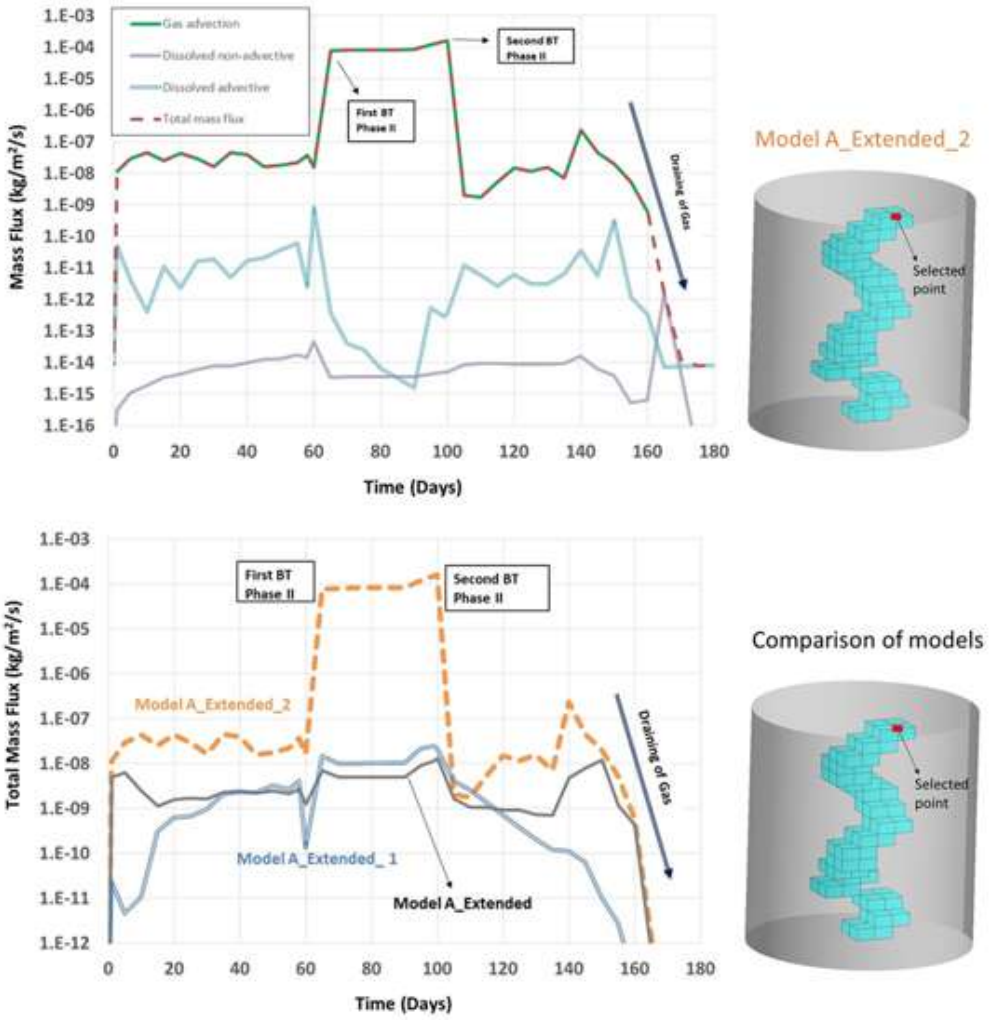

Figure 2.125: Mass fluxes in Model A_Extended_2 (above) and comparison of total mass fluxes for the different models (below).

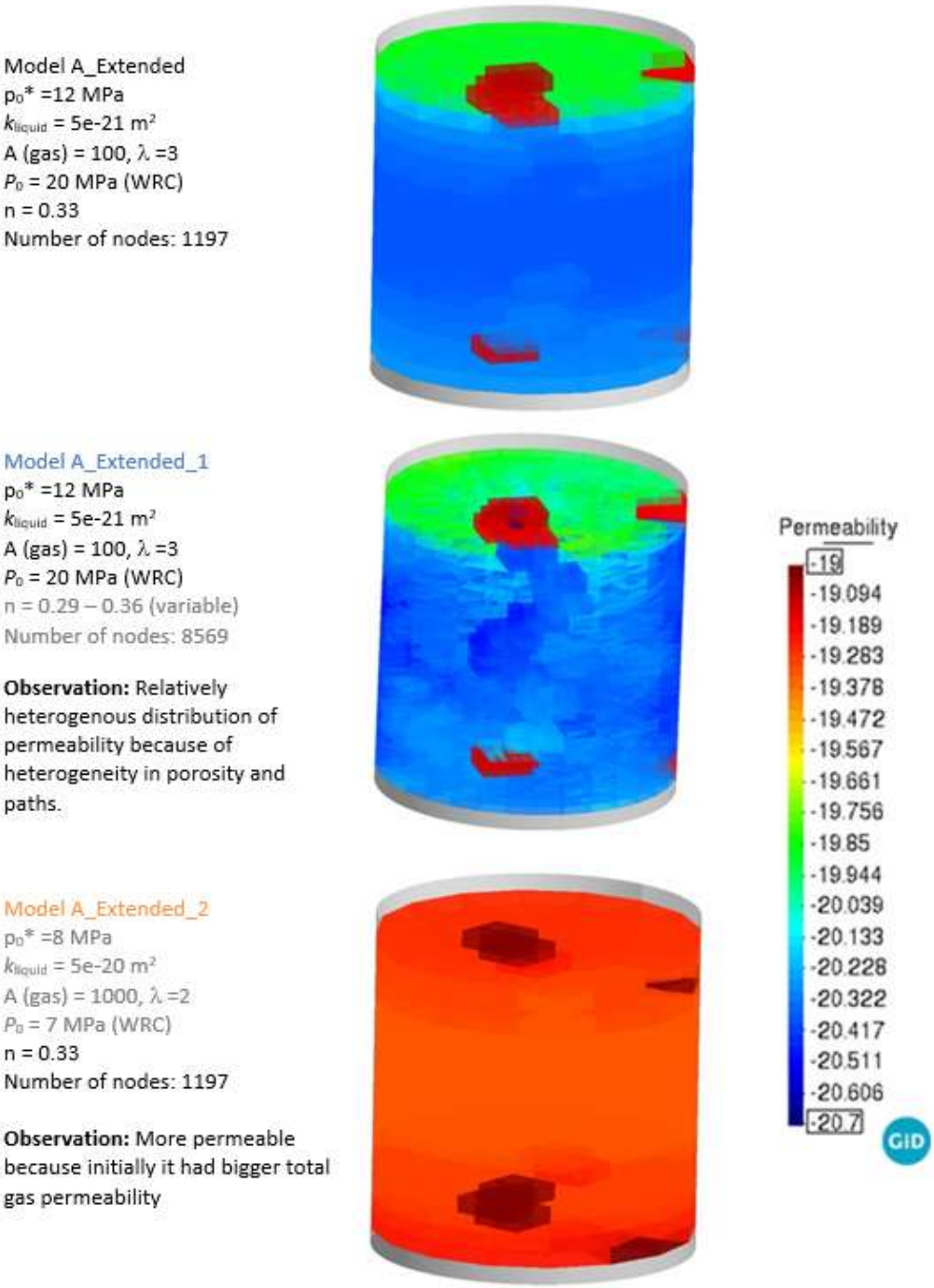

Figure 2.126: Distribution of permeability (logarithmic scale) in three models during first breakthrough (58 days later gas injection).

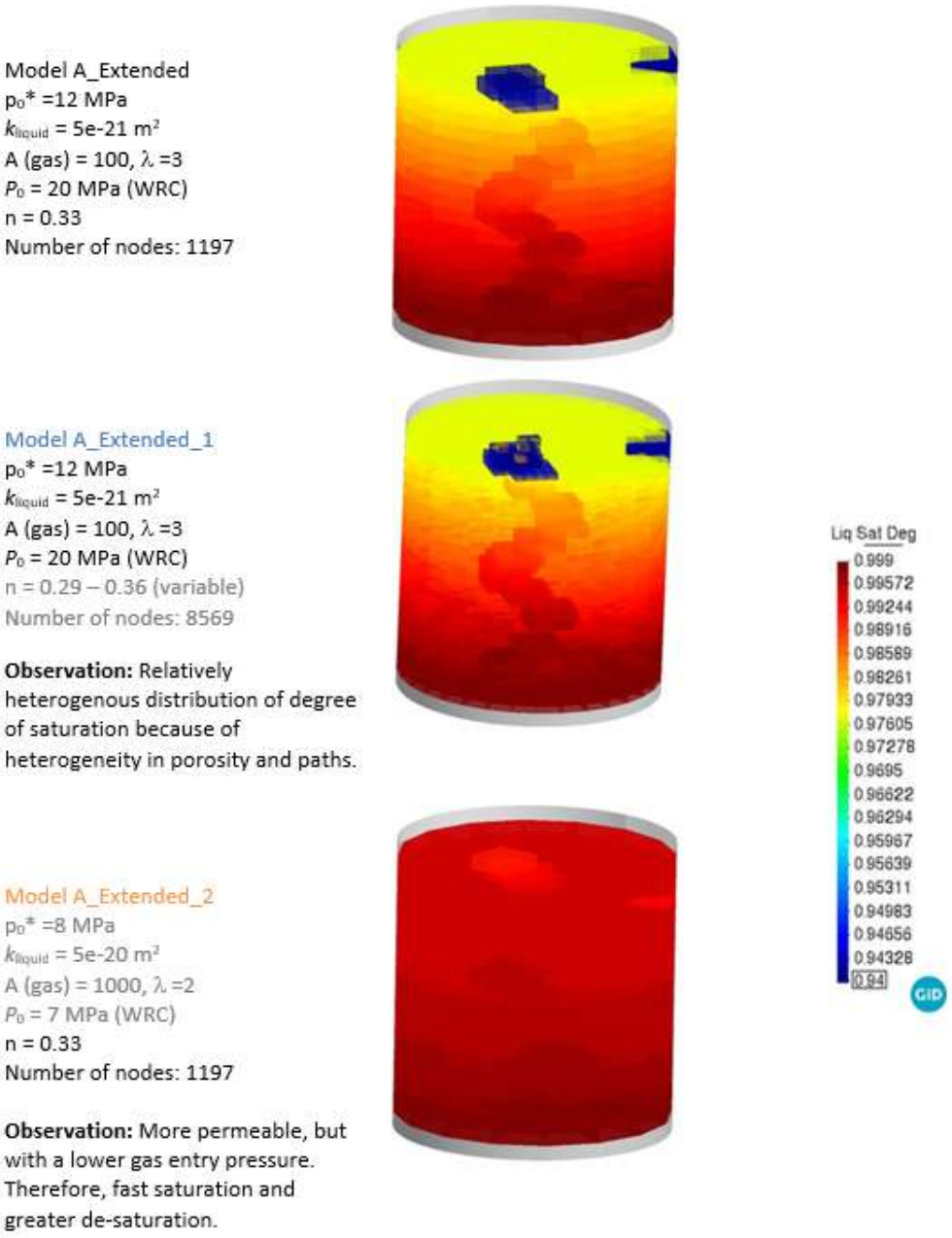

Figure 2.127: Distribution of liquid saturation degree in three models during first breakthrough (58 days later gas injection).

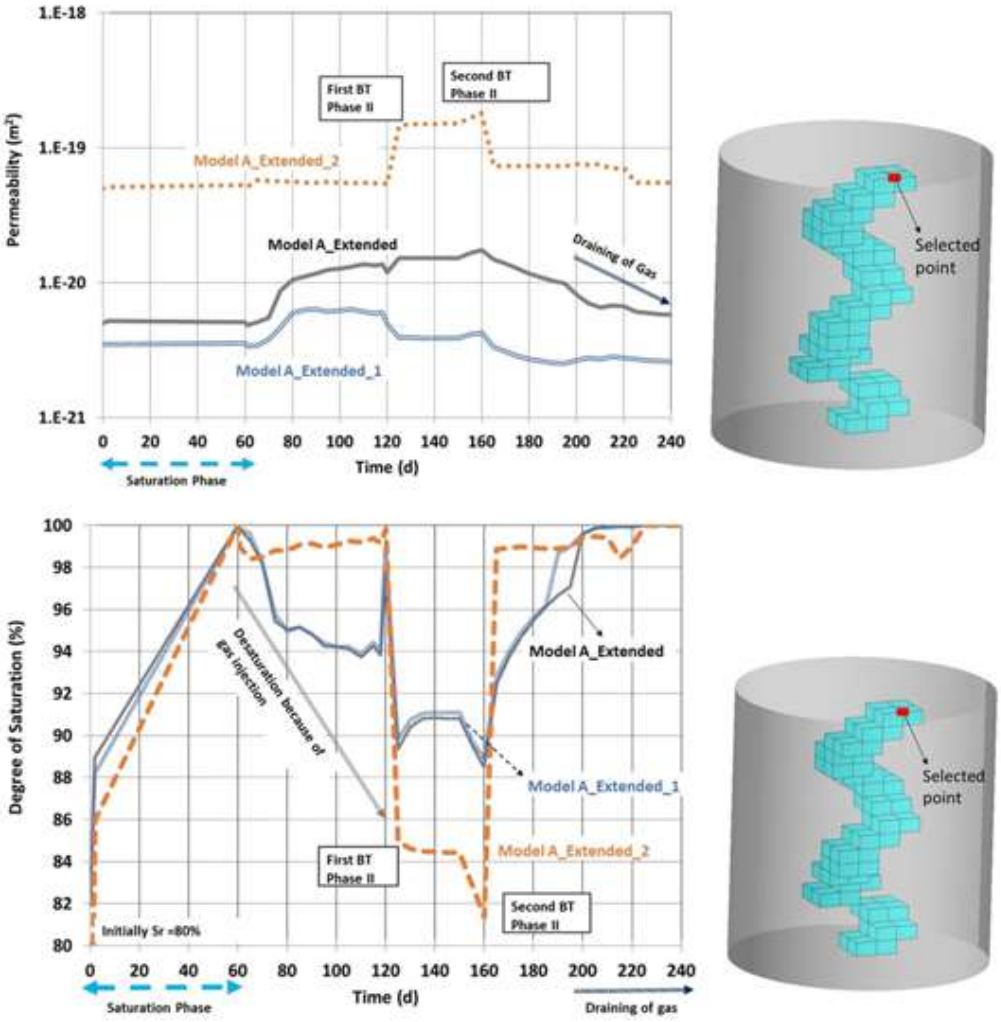

Figure 2.128: Comparison of permeability and degree of saturation evolutions in the models.

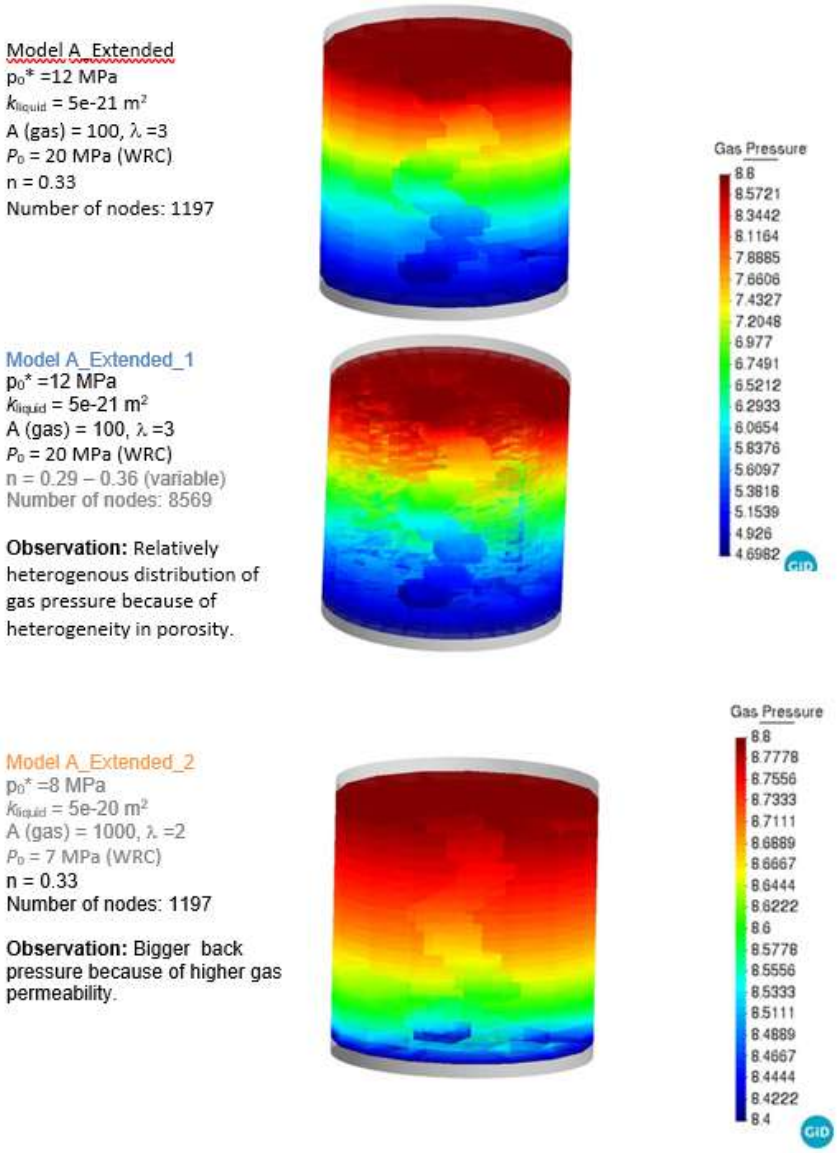

Figure 2.129: Distribution of gas pressure in three models during first breakthrough (58 days later gas injection).

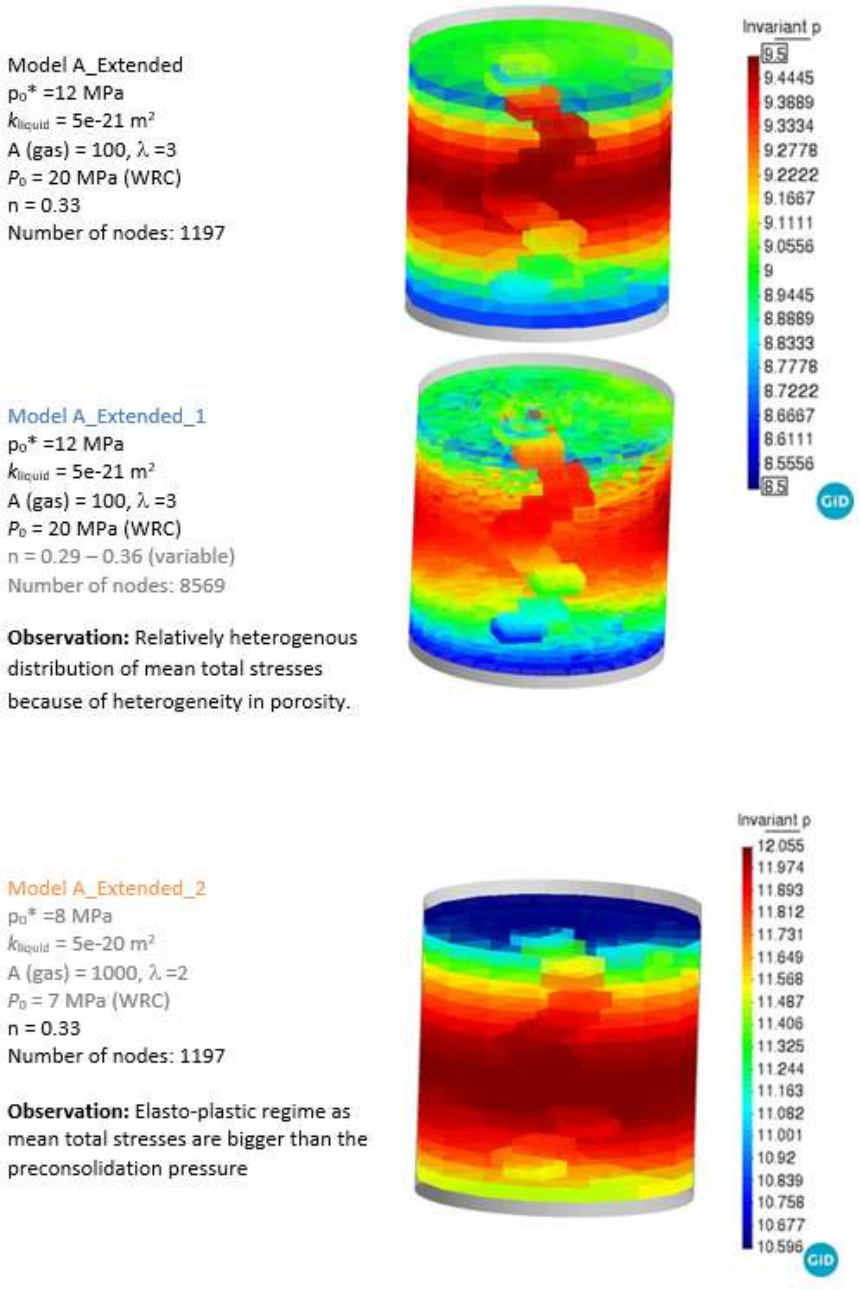

Figure 2.130: Distribution of mean total stresses in three models during first breakthrough (58 days later gas injection).

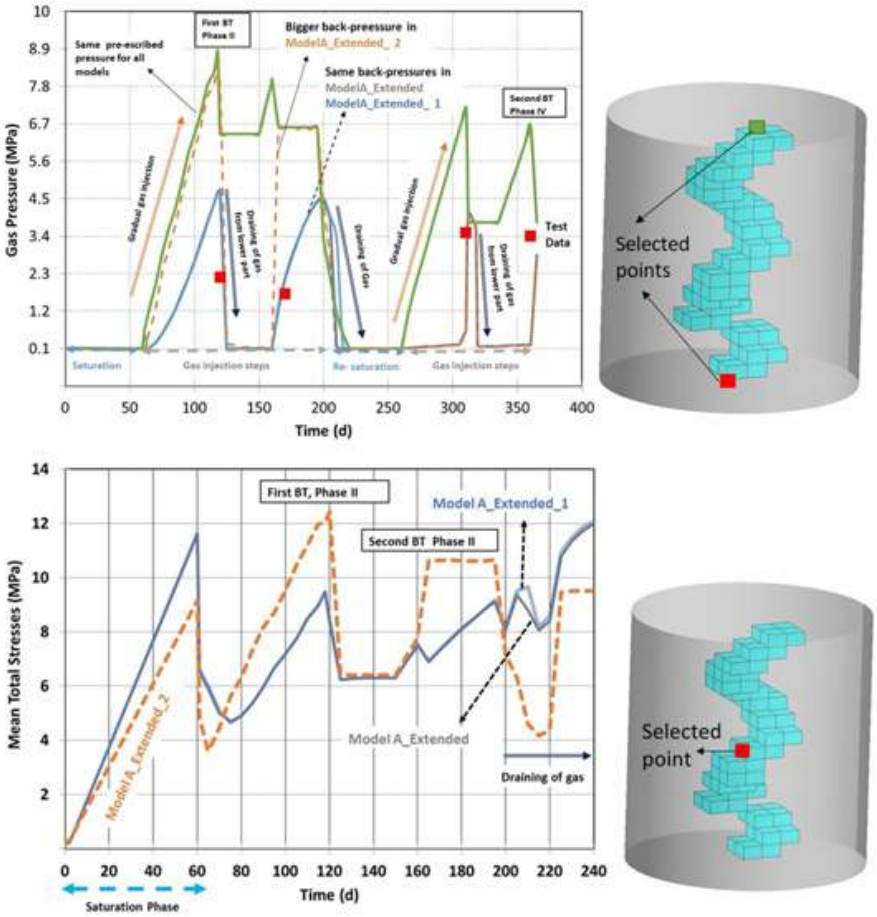

Figure 2.131: Comparison of gas pressure (above) and mean total stresses (below) in the models.

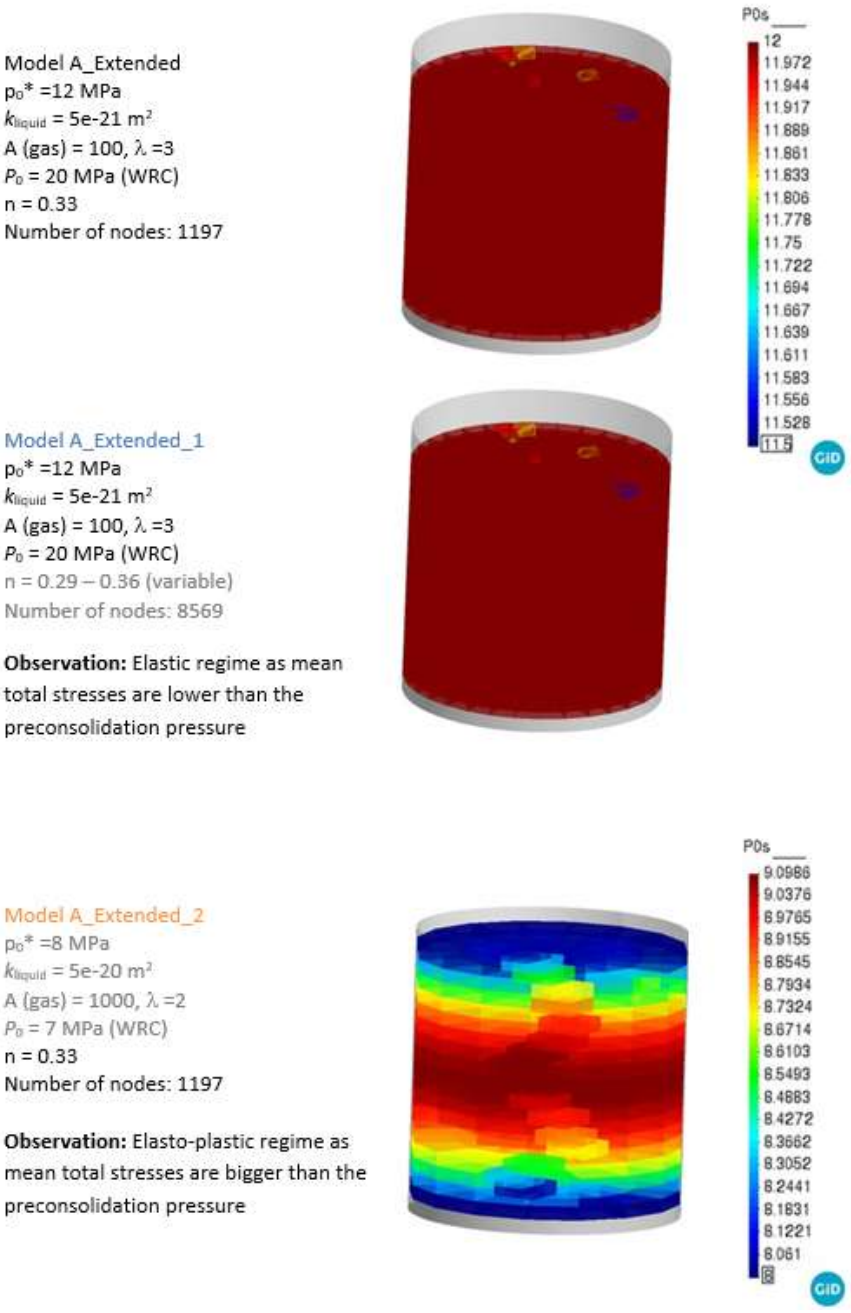

Figure 2.132: Distribution of pressure of pre-consolidation in three models during first breakthrough (58 days later gas injection).

2.5.7. Summary

In order to investigate gas transport process in bentonite barrier (FEBEX bentonite) and gas pathway development along the barrier; hydro-mechanical simulation of a breakthrough test (Gutierrez, 2018) has been performed. The objective of the modelling work was to simulate all phases of the test under proper boundary conditions, material model options and geometrical configuration.

BBM has been selected as a geo-mechanical model for the clay (FEBEX). In order to simulate increase in permeability during gas injection, cubic law for permeability has been used as a hydro-mechanical model for the gas flow pathways.

A full 3D geometry with different heterogeneity configurations (connected and unconnected paths), including porous stones, has been developed for the purpose of simulation of the test. One of the aims of the test was to simulate all processes (saturation, draining, gas injection, dismantling, etc.) taking place in the test.

A sensitivity analyses plan has been followed in order to improve model response and deal with test robustness and uncertainties. Table 2.30 summarizes objective, challenges, solutions and achievements of the modelling work.

Table 2.30: Summary, challenges and progress of the modelling work

Objective	• To investigate gas transport mechanism in FEBEX (initially unsaturated) material.
Challenges Limitations	• Mechanical Model : Using BBM in a 3D model with complex boundary conditions. • Boundary Conditions: Water/gas exchange procedure. Saturation and gas injection steps under the same 3D model. • Hydraulic Model: Verification and validation of heterogenous zones, preferential pathways and cubic law parameters.
Solutions Suggestions	• Preparation of a continues and layered geometry with structured mesh • Gradual gas injection and draining on the boundaries. • Follow a sensitivity analysis plan.
Sensitivity analyses	• Geometrical : Connected (Model A) and unconnected paths (Model B). • Time stepping : Prolongation of the test, including dismantling of the sample and re-saturation followed by new gas injection steps (Model A_Extended, Model B_Extended). • Hydro-mechanical model parameters: Variation of gas permeability, gas entry pressure; initial variable porosity and preconsolidation pressure (Model A_Extended_1 and Model A_Extended_2) • Computational: Refine of meshing, increasing number of elements (Model A_Extended_1)

Table 2.30: Summary, challenges and progress of the modelling work

Objective	• To investigate gas transport mechanism in FEBEX (initially unsaturated) material.
Achievements Progress	• HM Model**:** 3D modelling of a gas BT test on FEBEX with BBM and cubic law for permeability. • Full process: Saturation, draining, water/gas exchange, gas injection and gas/water exchange processes under the same 3D model. • Improvement of model response especially for Phase IV.

2.5.8. Key learning points

New knowledge acquired

It has been shown the possibility of modelling of gas breakthrough test with all experimental steps (saturation, gas injection, draining of gas, re-saturation and second gas injection) under a 3D full geometry by using complex hydro-mechanical models (cubic law for permeability and BBM as a mechanical model). The methodology can be applied to model other experiments and using other realizations of the heterogeneity field (based on imaging techniques for observation of real heterogeneity).

Impact of acquired knowledge

The model with heterogeneous zones (connected paths and/or unconnected paths) has been generated for a laboratory scale test. The model can be considered as a reference case and can be served to model in-situ and full scale gas injection tests under 3D geometries with complex hydro-mechanical models. The methodology used to generate heterogeneous zones and pathways can be used for upscaling.

Remaining knowledge gaps

The model is capable to predict test results. However, it considers arbitrarily random distribution of permeability zones (corresponding to realizations). By providing a better instrumentation and sensor data, imaging techniques, transparent walls, etc; permeability and porosity zones can be defined better.

Regarding material properties, it can also be interesting to incorporate double structure models (BExM) and geochemistry. In this way macro-porosity can play a key role on gas migration, and chemistry can have an influence on swelling capacity of the clay components.

Recommendations for the future

In this work, it was not possible to localize heterogeneous permeability fields as the sample was small and the instrumentation was limited. For this kind of tests, a better instrumentation is recommended. Also it is very important to collect realistic distributions of density or porosity for real samples before and after testing them.

There are two levels of heterogeneity observed during gas injection test. The first level of heterogeneity is associated with the variation of dry density (porosity) during the hydration. Gas BT pressures are associated with the final dry density (swelling pressure varies according to dry density) prior to gas injection

rather than the initial dry density. Therefore, hydration step shall be integrated in the modelling in order to improve the model predictions. The second level of heterogeneity is related to gas effective permeability. In intact clay (no advection of free gas), gas permeability and WRC is porosity dependent. In contrast, gas permeability and WRC is strain dependent in dilatant pathways. The magnitude of the apertures in dilatant pathways is variable. Therefore, at least two different gas flow pathways with different aperture characteristics shall be integrated into model. An elasto-plastic model such as BBM is required not only to reproduce development of swelling pressures during hydration part but also to simulate possible irreversible strains induced by gas injection under the heterogenous model configuration.

References

Alonso EE, Gens A and Josa A (1990) A constitutive model for partially saturated soils. Géotechnique 40(3): 405-430. 1990. pp. 405-430.

Enresa (2000) FEBEX Project. Full-scale engineered barriers experiment for a deep geological repository for high level radioactive waste in crystalline host rock. Enresa, Madrid, Spain. Final report, 1/2000.

Enresa (2006) Full-scale engineered barriers experiment. Enresa. Madrid. Spain. Updated final report 1994-2004. Technical publication 05-0/2006.

Gens A, Sánchez M and Guimaraes LN et al. (2009) A full-scale in situ heating test for high-level nuclear waste disposal: observations, analysis and interpretation. s.l.: Géotechnique, 59(4): 377-399, 2009. pp. 377-399.

Olivella S, Carrera J, Gens A & Alonso EE (1994) Nonisothermal multiphase flow of brine and gas through saline media. Barcelona, Spain. Transport in Porous Media, 1994. 271–293.

Olivella S. And E.E. Alonso, Gas flow through clay barriers, 2008, Geotechnique 58, No. 3, 157–176 [doi: 10.1680/geot.2008.58.3.157]

Gutiérrez Vanesa Transporte de gas en materiales de barrera, PhD dissertation, 2018.

Toprak E, Olivella S and Pintado X, (2020) Modelling engineered barriers for spent nuclear fuel repository using a double-structure model for pellets. Environmental Geotechnics, [doi: 10.1680/jenge.17.00086.